Mediterranean Sea Production Centre
MEDSEA_REANALYSIS_BIO_006_008

Issue: 2.4

Contributors: A. Teruzzi, G. Cossarini, S. Salon, G. Bolzon, P. Lazzari, L. Feudale

Approval date by the CMEMS product quality coordination team: 29/05/2019

CHANGE RECORD

When the quality of the products changes, the QuID is updated and a row is added to this table. The third column specifies which sections or sub-sections have been updated. The fourth column should mention the version of the product to which the change applies.

Issue	Date	§	Description of Change	Author	Validated By
1.0	26/01/2016	all	First version of document at CMEMS V2	G. Cossarini, S. Salon, G. Bolzon, A. Teruzzi, P. Lazzari, E. Clementi	E. Clementi
1.1	04/04/2016	IV	Revised version after Acceptance Review Report and with assimilation of the updated V2 ESA-CCI data set	G. Cossarini, S. Salon, G. Bolzon, A. Teruzzi, P. Lazzari, E. Clementi	E. Clementi
2.0	18/01/2017	all	Version of document at CMEMS V3	G. Cossarini, S. Salon, G. Bolzon, A. Teruzzi, P. Lazzari	
2.1	07/02/2017	all	Updates of the version of document at CMEMS V3	G. Cossarini, S. Salon, G. Bolzon, A. Teruzzi, P. Lazzari	
2.2	16/02/2018	all	Updates of the version of document at CMEMS V4	G. Cossarini, S. Salon, G. Bolzon, A. Teruzzi, P. Lazzari, L. Feudale	Mercator Ocean
2.3	21/01/2019	all	Updates of the version of document for temporal extension Q1 2019	A. Teruzzi, G. Cossarini, S. Salon, G. Bolzon, P. Lazzari, L. Feudale	
2.4	3/09/2019	all	Updates of the version of document for temporal extension Q4 2019	A. Teruzzi, G. Cossarini, S. Salon, G. Bolzon, P. Lazzari, L. Feudale	

TABLE OF CONTENTS

I EXECUTIVE SUMMARY

I.1 Products covered by this document

This document describes the quality of the product MEDSEA_REANALYSIS_BIO_006_008, the multi-year product of the biogeochemical state of the Mediterranean Sea for the period 1999-2018 produced by the CMEMS-Med-MFC-Biogeochemistry for Q4 2019. The MED Biogeochemistry reanalysis product includes 3D monthly fields at 1/16° horizontal resolution (which for the Mediterranean basin ranges from 5 km at 45°N to 6 km at 30°N) of 8 variables grouped in 4 datasets:

PFTC: chlorophyll and phytoplankton carbon biomass;

NUTR: phosphate and nitrate;

BIOL: dissolved oxygen concentrations and net primary production;

CARB: ocean pH (reported on Total Scale) and ocean pCO2.

Citation: Teruzzi A., Cossarini G., Lazzari P., Salon S., Bolzon G., Crise A., Solidoro C. (2016). "Mediterranean Sea biogeochemical reanalysis (CMEMS MED REA-Biogeochemistry 1999-2015)". [Data set]. Copernicus Monitoring Environment Marine Service. DOI: https://doi.org/10.25423/MEDSEA_REANALYSIS_BIO_006_008

I.2 Summary of the results

The quality of the MED biogeochemistry reanalysis MEDSEA_REANALYSIS_BIO_006_008 from 01/01/1999 to 31/12/2018 has been assessed by comparison with independent data (observational in-situ datasets), semi-independent data (satellite datasets) and literature estimates. The main results of the quality product assessment are summarized in the following points:

Chlorophyll: Results give evidence of the model capability of reproducing spatial patterns, seasonal cycle and inter-annual variability. The model chlorophyll BIAS is order 10^{-3} mg/m^3 in open sea, with minimum values in summer in the eastern sub-basins, while it increases to 10^{-1} mg/m^3 in the coastal areas, now covered by the data assimilation. For the open sea, western sub-basins are characterized by higher uncertainty and variability (estimated by the RMSD) than eastern ones. In the coastal areas the uncertainty rises up to 1 mg/m^3 in areas more affected by river inputs and shelf dynamics, where model underestimates the high values of chlorophyll.

Phytoplankton carbon biomass: No validation metrics are feasible due to the lack of a reliable reference dataset. Consistency of the model formulation (discussed in several scientific papers) and validation of phytoplankton chlorophyll provide an indirect proof of the accuracy for this variable.

Phosphate: Uncertainties at basin scale (measured in terms of RMSD) are generally around 0.03 and 0.07 mmol/m^3 at the upper and deep layers, respectively. Simulated general basin-wide gradients and vertical profile shapes are consistent with observations (correlation higher than 0.8).

Nitrate: Major horizontal spatial gradients (sub-basin wide patterns) and vertical are consistent with observations (correlations up to 0.7). Uncertainties at basin scale are of the order of 0.5 and 1.5

mmol/m^3 at the upper and deep layers, respectively. Western Mediterranean Sea (e.g. North Western sub-basin in the upper layers) and intermediate layer (e.g. Alboran Sea at 300-600 m) show the highest uncertainty (up to 4 mmol/m^3).

Oxygen: Uncertainties are order 10-15 mmol/m^3 at basin scale. Western Mediterranean Sea areas (e.g. Alboran, South Western sub-basins) might be affected by a not proper setting of the boundary conditions at the Atlantic buffer.

Net primary production: Comparison with literature shows that the reanalysis simulation consistently reproduces basin-scale and sub-basin-scale estimates.

pH and pCO2: Uncertainties of ocean acidity (pH at in-situ conditions and reported in total scale) and of partial pressure of carbon dioxide in sea water (pCO2) have been computed indirectly using the error propagation approach and the uncertainty of the alkalinity and dissolved organic carbon (DIC) for which observations are available. The comparison with observations shows that the reanalysis satisfactorily reproduces the main spatial patterns and vertical dynamics of the carbonate system variables. The overall estimate of pH and pCO2 uncertainty is 0.048 and 48.1 µatm, respectively.

Important notice: *This reanalysis assimilates surface chlorophyll concentration data from both open sea and coastal areas. Chlorophyll satellite data are the reprocessed data OCEANCOLOUR_MED_CHL_L3_REP_OBSERVATIONS_009_073 (updated on April 2016) for the period January 1999 to August 2015 and the near real time data OCEANCOLOUR_MED_CHL_L3_NRT_OBSERVATIONS_009_040 for the period September 2015 to December 2018. This reanalysis uses the physical forcing (currents, temperature and salinity, wind and short wave radiation) MEDSEA_REANALYSIS_PHYS_006_004.*

I.3 Estimated Accuracy Numbers

Chlorophyll [mg/m^3]				
	RMSD		BIAS	
	win	sum	win	sum
OPEN SEA				
Mod-Sat	0.067	0.024	-0.001	-0.004
log_{10}(Mod)-log_{10}(Sat)	0.152	0.122	-0.020	-0.023
COASTAL AREAS				
Mod-Sat	0.577	0.860	0.159	0.155
log_{10}(Mod)-log_{10}(Sat)	0.257	0.294	0.090	0.148

Table I.1. Mean RMSD and BIAS (model minus satellite) of surface chlorophyll [mg/m^3] over the open sea and coastal areas of the Mediterranean Sea. Winter corresponds to January to April, summer corresponds to June to September.

	RMSD							
Layers (m)	**0-10**	**10-50**	**50-100**	**100-150**	**150-300**	**300-600**	**600-1000**	**CORR.**
Phosphate [mmol/m^3]	0.03	0.02	0.03	0.04	0.08	0.07	0.09	0.83
Nitrate [mmol/m^3]	0.50	0.42	0.46	1.00	1.35	1.77	1.67	0.68
Oxygen [mmol/m^3]	12.93	17.57	18.86	16.36	10.58	11.51	11.69	0.47

Table I.2. Mean RMSD and correlation of phosphate, nitrate and oxygen estimated by comparing the reanalysis and in-situ 1999-2014 observations.

Variables	Uncertainty
pH	0.048
pCO2 [µatm]	48.1

Table I.3. Uncertainty of pH (total scale and in-situ condition) and partial pressure of carbon dioxide in seawater (pCO2) for the surface layer, estimated indirectly by error propagation approach using uncertainty of DIC and Alkalinity.

II PRODUCTION SYSTEM DESCRIPTION

II.1 Production centre details

Production centre name: OGS, IT

Production system name: Mediterranean Sea Reanalysis biogeochemistry (CMEMS name: MEDSEA_REANALYSIS_BIO_006_008)

Description

The biogeochemical reanalysis for the Mediterranean Sea is produced by the OGS Production Unit by means of the MedBFM1 model system. MedBFM1 includes the transport model OGSTMv2.0 coupled with the biogeochemical model BFMv2.1 and the surface chlorophyll data assimilation module 3DVAR-BIOv2.1. The data assimilation module has been upgraded with respect to the previous version in order to assimilate surface chlorophyll concentration also from coastal areas. In this reanalysis, OGSTMv2.0 was driven by physical forcing fields produced as output by the Med-MFC-Currents model managed by the INGV Production Unit. The ESA-CCI database of surface chlorophyll concentration estimated by satellite and delivered within CMEMS-OCTAC managed by GOS-ISAC-CNR was used for data assimilation. Figure II.1 shows the layout of the MedBFMv1 biogeochemical model system.

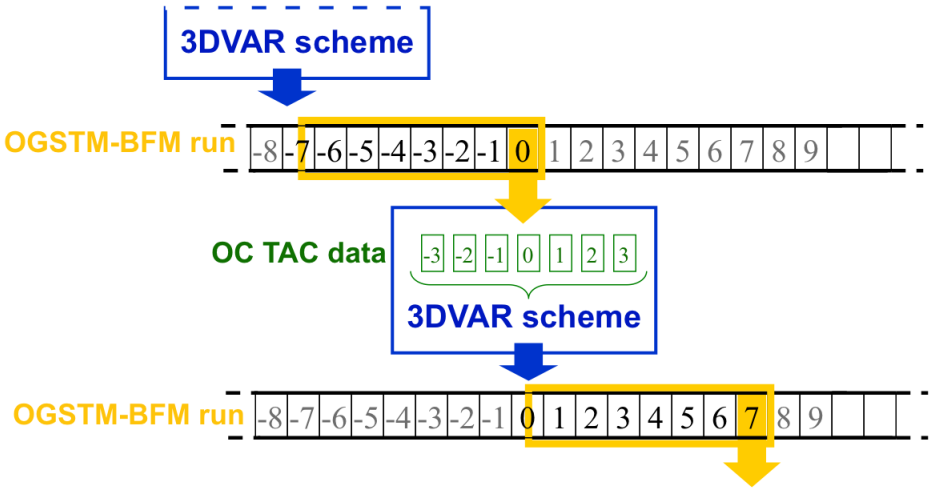

Figure II.1. Scheme of the functioning of the Med-MFC-biogeochemistry system for the reanalysis: blue boxes represent the 3DVAR-BIO assimilation scheme, the orange box represents the days of the run of coupled model OGSTM-BFM, the orange arrow is the mean daily forecast used in the assimilation, green boxes represent the 7 days of satellite chlorophyll fields used to produce a mean field that is assimilated in the reanalysis.

The Med-MFC-biogeochemistry reanalysis run is composed by the following steps, which are repeated every week for the period 1st January 1999 – 31st December 2018 (Figure II.1):

1. Pre-processing: pre-processing of the physical forcings (perform a quality control and a cut in the Atlantic sector) and of the satellite chlorophyll observations (spatial interpolation, quality check and 7-day average).

2. Data assimilation: a 3DVAR scheme for the assimilation of surface chlorophyll observations in open sea and coastal areas is performed (details on the assimilation scheme are provided in Teruzzi et al., 2014, 2018, 2019).
3. Model run: the biogeochemical OGSTM-BFM model is run for seven days starting from 12pm of the first day of analysis.
4. Post processing: the model output is processed in order to obtain the monthly CMEMS products.

II.2 Description of the MedBFM1 model system

The Med-biogeochemistry system is based on the MedBFM1, which includes the 3DVAR-BIOv2.1 assimilation module and the OGSTMv2.0 and BFMv2.1 models (Lazzari et al., 2010, 2012, 2016; Teruzzi et al., 2014, 2018, 2019; Cossarini et al., 2015, and references thereby).

OGSTMv2.0 and BFMv2.1 are respectively designed with a transport model based on the OPA system and a biogeochemical reactor featuring the Biogeochemical Flux Model (BFM), while 3DVAR-BIOv2.1 is the data assimilation scheme for the correction of phytoplankton functional type variables (Figure II.2; Lazzari et la., 2012 and https://cmcc-foundation.github.io/www.bfm-community.eu/ for details on BFM).

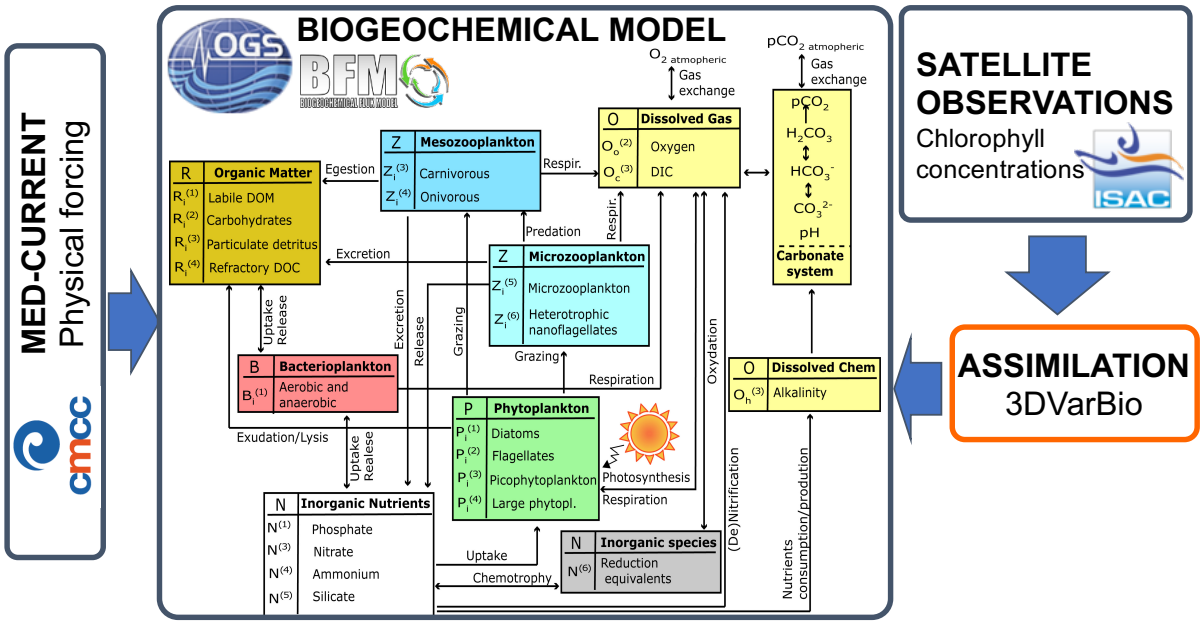

Figure II.2. The Med-biogeochemistry model system and interfaces with other components of Copernicus system.

The transport OGSTM model is a modified version of the OPA 8.1 transport model (Foujols et al., 2000), which resolves the advection, the vertical diffusion and the sinking terms of the tracers (biogeochemical variables). The meshgrid is based on 1/16° longitudinal scale factor and on 1/16°cos(ϕ) latitudinal scale factor. The vertical meshgrid accounts for 72 vertical z-levels: 25 in the first 200 m depth, 31 between 200 and 2000 m, 16 below 2000 m. The temporal scheme of OGSTM-BFM is an explicit forward time scheme for the advection and horizontal diffusion terms, whereas an

implicit time step is adopted for the vertical diffusion. The sinking term is a vertical flux which acts on a sub-set of the biogeochemical variables (particulate matter and phytoplankton groups). Sinking velocity is fixed for particulate matter and dependent on nutrients for two phytoplankton groups (diatoms and dinoflagellates).

The physical dynamics that are off-line coupled with the biogeochemical processes are pre-computed by the MED-PHY which supplies the temporal evolution of the fields of horizontal and vertical current velocities, vertical eddy diffusivity, potential temperature, salinity, in addition to surface data for solar shortwave irradiance and wind stress (see section on upstream data and boundary conditions for further details).

The features of the biogeochemical reactor BFM (Biogeochemical Flux Model) have been chosen to target the energy and material fluxes through both “classical food chain” and “microbial food web” pathways (Thingstad and Rassoulzadegan, 1995), and to take into account co-occurring effects of multi-nutrient interactions. Both of these factors are very important in the Mediterranean Sea, wherein microbial activity fuels the trophodynamics of a large part of the system for much of the year and both phosphorus and nitrogen can play limiting roles (Krom et al., 1991; Bethoux et al., 1998). The model presently includes nine plankton functional types (PFTs). Phytoplankton PFTs are diatoms, flagellates, picophytoplankton and dinoflagellates. Heterotrophic PFTs consist of carnivorous and omnivorous mesozooplankton, bacteria, heterotrophic nanoflagellates and microzooplankton.

BFM model describes the biogeochemical cycles of 4 chemical compounds: carbon, nitrogen, phosphorus and silicon through the dissolved inorganic, living organic and non-living organic compartments. Nitrate and ammonia are considered for the dissolved inorganic nitrogen. The non-living compartments consists of 3 groups: labile, semilabile and refractory organic matter. The last two are described in terms of carbon, nitrogen, phosphorus and silicon contents. The model is fully described in Lazzari et al. (2012, 2016), where it was corroborated for chlorophyll, primary production and nutrients in the Mediterranean Sea for a 1998-2004 simulation.

The BFM model is also coupled to a carbonate system model (Cossarini et al., 2015), which consists of two prognostic state variables: alkalinity (ALK) and dissolved inorganic carbon (DIC). DIC evolution is driven by biological processes (photosynthesis and respiration, and precipitation and dissolution of CaCO3) and physical processes (exchanges at air-sea interface and dilution-concentration due to evaporation minus precipitation process). Alkalinity evolution is affected by biochemical processes that alter the ions concentration in sea water (nitrification, denitrification, uptake and release of nitrate, ammonia and phosphate by plankton cells, and precipitation and dissolution of CaCO3). DIC exchange at the air-sea is resolved by computing the seawater pH, pCO2 and gas transfer formula (OCMIP II model, Orr et al., 1999).

II.3 Description of Data Assimilation scheme

The data assimilation of surface chlorophyll concentration is performed once a week during the reanalysis run through a variational scheme (3DVAR-BIO, see details on Teruzzi et al., 2014, 2018, 2019). The surface chlorophyll concentrations consist of satellite observations produced by OCTAC based on the ESA-CCI data. The present version of 3DVAR-BIO assimilates chlorophyll concentration over the whole domain including both the open sea and the coastal areas. The data assimilation corrects the four phytoplankton functional groups included in the OGSTM-BFM. The 3DVAR-BIO scheme decomposes the error covariance matrix using a sequence of different operators that account

separately for the vertical covariance ($\mathbf{V_V}$), the horizontal covariance ($\mathbf{V_H}$) and the covariance among biogeochemical variables ($\mathbf{V_b}$).

$\mathbf{V_V}$ is defined by a set of synthetic profiles that are evaluated by means of an Empirical Orthogonal Function (EOF) decomposition. EOFs vertical profiles for coastal and open sea assimilation have been calculated using the chlorophyll fields produced by the 1999–2014 Mediterranean Sea biogeochemistry V2 reanalysis (CMEMS-Med-MFC-BIO-006-008). In particular, in areas with depth greater than 200 m, the EOFs have been obtained with the approach described in Teruzzi et al. (2014); while, in areas with depth lower than 200 m of each sub-basin, a k-means analysis identifies two regions (k-regions) with different chlorophyll dynamics and a set of EOFs has been evaluated for each k-region and each month. Finally, the monthly EOFs of sub-basins and k-regions have been calibrated based on the local (i.e. domain gridpoint) surface estimate of the model error. As a result, the $\mathbf{V_V}$ operator consists of a set of EOFs profiles for each grid point with common vertical shape within each sub-basin and each k-region.

$\mathbf{V_H}$ is built using a Gaussian parameterization whose correlation radius modulates the smoothing intensity and the horizontal spatial areas influenced by the operator (Dobricic and Pinardi, 2008). The $\mathbf{V_H}$ operator has been made non uniform and anisotropic for the coastal areas (areas with depth lower than 200 m). In particular, the effects of morphological features and physical currents, which are relevant on the horizontal propagation of biogeochemical dynamics in coastal area, are integrated by two new fields of non-uniform correlation lengths, Lx and Ly. The Lx and Ly correlation length scales vary in space and have been computed proportional to the inverse of the salinity gradient along the longitude and the latitude, respectively. The salinity field used to define the correlation radii is the mean salinity of the CMEMS Mediterranean Sea Physics reanalysis V2 (CMEMS-Med-MFC-PHY-006-004). In areas with water column depth greater than 200 m the correlation length has been set equal to 10 km (i.e. unchanged respect to the previous V2 version).

$\mathbf{V_b}$ operator maintains the relative composition among the phytoplankton groups and preserves the physiological status of the phytoplankton cells. In particular the internal ratios of chlorophyll-carbon and chlorophyll-nutrient are preserved, and the innovations are proportionally applied to all of the components of the phytoplankton functional types. However, in case of positive innovation Vb operator is relaxed in order to keep the optimal growth condition, preserving the internal contents of nutrients or increasing it as necessary. Moreover, positive innovation at depths with no light and nutrient internal ratio very far from optimal ratios (starvation stage of phytoplankton groups) is not applied.

The assimilation scheme updates the initial conditions every week during the simulation run according to the following steps (Figure II.1):

1. a 7-day [from T-3 to T+3] average chlorophyll map is computed and spatially interpolated on the model grid;

2. the misfit is evaluated as the difference between the satellite chlorophyll and the simulated sum of the four phytoplankton type chlorophylls at the central day of the 7-day period [T0];

3. the 3D-VAR provides the innovation for the four phytoplankton group variables;

4. the new initial conditions (analysis) are produced, and the setup for the simulation of the next seven days is prepared;

5. a new 7-day period is simulated [from T+1 to T+7] using the updated initial conditions, plus the physical and boundary conditions.

II.4 Upstream data and boundary conditions

The CMEMS–MED-MFC-Biogeochemistry system uses the following upstream data:

1. Daily off-line coupled physical forcing and atmospheric forcing are those of the official product MEDSEA_REANALYSIS_PHYS_006_004 version V4.

2. Data assimilation uses satellite surface chlorophyll from the dedicated CMEMS-OCTAC products OCEANCOLOUR_MED_CHL_L3_REP_OBSERVATIONS_009_073 version V2 (released in April 2016) for the period 1/1/1999 to 31/8/2015, and OCEANCOLOUR_MED_CHL_L3_NRT_OBSERVATIONS_009_040 version V3 for the period 1/9/2015 to 31/12/2018. The consistency between the two satellite products has been resolved by applying monthly varying maps of bias correction computed on the overlapping period of the two products (Figure II.3).

3. Initial conditions: the nutrient pools (nitrate, phosphate, silicate) and dissolved oxygen for the BFM biogeochemical model were initialised using the MEDAR MEDATLAS 2002 data set (Crise et al., 2003). In particular, the extracted data include measurements of dissolved oxygen (from 1948 to 2002), nitrate (from 1987 to 2002), phosphate (from 1987 to 2002) and silicate (1987 to 2002). A vertical nutrient profile was assigned uniformly to each of the eleven regions reported in Crise et al. (2003). The other biogeochemical state variables were homogeneously initialised in the photic layer (0–200 m) according to the standard BFM values and with lower values in the deeper layers. The initial conditions of the variables of the carbonate system (dissolved inorganic carbon and alkalinity) are from a previous run as described in Cossarini et al. (2015). The model spin-up consists of a four years hindcast run starting from 1st January 1995 using the physical forcing (MEDSEA_REANALYSIS_PHYS_006_004) available for the period. The assimilation of the available satellite data is done since January 1st 1999, thus the official CMEMS product is made available starting from the 1st January 1999.

4. Boundary conditions (BCs) of the reanalysis run at Gibraltar Strait, Dardanelles, rivers and atmosphere deposition are provided as following:

   4.1. A Newtonian dumping term regulates the Atlantic buffer zone western of the Strait of Gibraltar, where the tracer concentrations are relaxed to the seasonally varying profiles. Seasonal profiles of phosphate, nitrate, silicate, dissolved oxygen are derived from climatological MEDAR-MEDATLAS data measured outside Gibraltar. For ALK and DIC, the Atlantic buffer profiles are obtained from the recent dataset (Huertas et al., 2009; de la Paz et al., 2011; Alvarez et al., 2014).

   4.2. Atmospheric deposition rates of inorganic nitrogen and phosphorus were set according to the synthesis proposed by Ribera d'Alcalà et al. (2003) and based on measurements of field data (Loye-Pilot et al., 1990; Guerzoni et al., 1999; Herut and Krom, 1996; Cornell et al., 1995; Bergametti et al., 1992). Atmospheric deposition rates of nitrate and phosphate were assumed to be constant in time during the year, but with different values for the western (580 Kt Nyr^{-1} and 16 Kt Pyr^{-1}) and eastern (558 Kt Nyr^{-1} and 21 Kt Pyr^{-1}) sub-basins. The rates were calculated by averaging the "low" and "high" estimates reported by Ribera d'Alcalà et al. (2003).

   4.3. Nutrient loads from rivers and other coastal nutrient sources were based on the reconstruction of the spatial and temporal water discharge variability estimated following the method described by Ludwig et al. (2009). These values are based on

available field data for nutrient concentrations, climate parameters that have been made available since the early 1960s. The nutrient discharge rates for the major rivers (Po, Rhone, Nile and Ebro) are climatological but take into account seasonal variability on a monthly scale and are calculated on the basis of direct observations. All other inputs are treated as constants throughout the year due to a lack of data.

4.4. Terrestrial inputs of ALK and DIC are derived with a procedure based on two phases. In the first phase the typical concentration of ALK and DIC per water mass are computed for 10 macro coastal areas covering the entire Mediterranean Sea coastline (as defined by Ludwig et al., 2009). In the second phase the total terrestrial input of mass of ALK and DIC is derived by multiplying the estimates of water discharge (Ludwig et al., 2009) by the concentration derived in the phase 1. The Dardanelles inputs where considered as river inputs (Somot et al., 2008): also in this case the total inflow was derived considering typical water mass concentration of ALK and DIC for Marmara Sea (Chopin-Montegut, 1993) multiplied by the net water mass fluxes. Atmospheric pCO2 concentration is set equal to the yearly average measured at the Lampedusa station (Artuso et al., 2009) between 1992 and 2017 (http://cdiac.ess-dive.lbl.gov/ftp/trends/co2/lampedus.co2) with the present-day values extrapolated by linear regression..

4.5. Surface evaporation-precipitation flux, which affects ALK and DIC by producing a dilution or concentration, was implemented as a virtual flux at the surface layer. The evaporation-precipitation flux, provided as monthly variable climatology, was corrected in order to be balanced with Dardanelles, Gibraltar Straits, and fresh water budget.

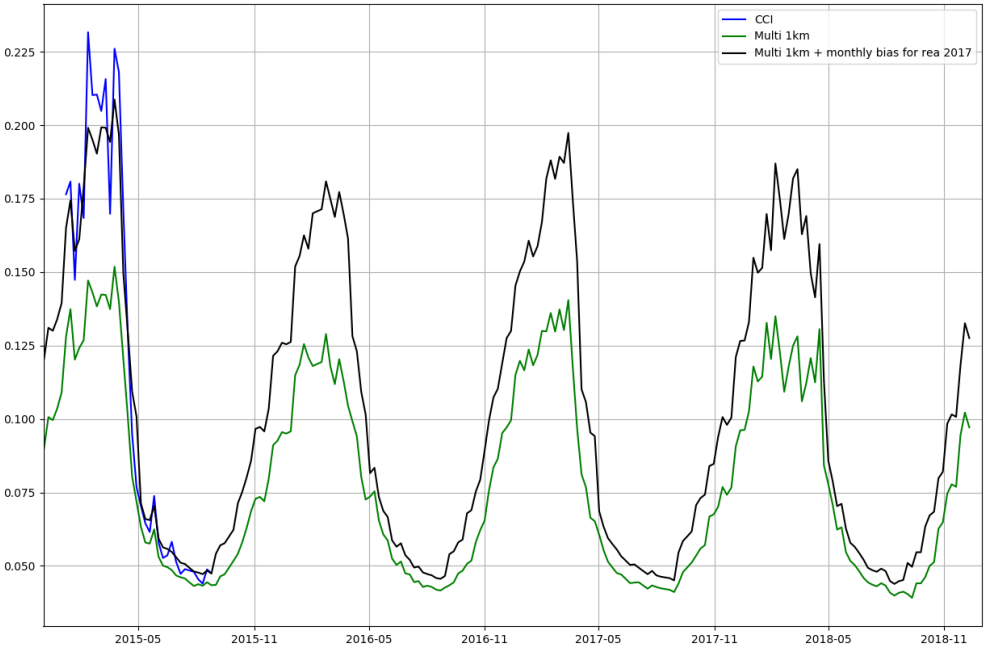

Figure II.3. Time series of mean satellite chlorophyll over the Mediterranean Sea [mg chl/m^3]. Blue: OCEANCOLOUR_MED_CHL_L3_REP_OBSERVATIONS_009_073 version V2; Green: OCEANCOLOUR_MED_CHL_L3_NRT_OBSERVATIONS_009_040 version V3; Black: bias corrected chlorophyll concentration used for the Sep2015-Dec2018 data assimilation.

III VALIDATION FRAMEWORK

The products assessed are chlorophyll, net primary production, phosphate, nitrate, oxygen, pH, pCO2 (see Table III.1).

Model chlorophyll data are compared with semi-independent data (ESA-CCI satellite chlorophyll downloaded from CMEMS OCTAC) using metrics that refer to the "misfits" computed as the differences between satellite chlorophyll (7-days composite map) and the model forecast at the time of the data assimilation execution (every 7 days). The metrics used are the BIAS and the Root Mean Square (RMS) of the differences between model output and observation, computed monthly for the Mediterranean Sea and selected sub-basins (Figure III.1), and reported as time series. Independent in situ observations of chlorophyll concentration along the Italian coast in 2013 (monthly measurements in more than 300 stations, Figure III.4) provided by the Italian National Institute for Environmental Protection and Research (ISPRA) are used to assess chlorophyll in the coastal areas. This dataset is used to evaluate the effect of the new data assimilation scheme that integrates coastal and open-sea areas satellite chlorophyll data.

Model net primary production data are compared with literature data based on multi-annual simulation (Lazzari et al., 2012), satellite model (Colella, 2006), in-situ estimates (Siokou-Frangou et al., 2010).

Model phosphate and nitrate data are compared with the World Ocean Atlas 2013 database at basin-scale for a series of vertical layers (0-10, 10-30, 30-60, 60-100, 100-150, 150-300 m).

Model phosphate, nitrate and dissolved oxygen data are compared with available moorings and vessels from OGS National Oceanographic Data Center (NODC-OGS) dataset (Table III.2 and Figure III.2) for selected sub-basins (Figure III.1). The NODC-OGS dataset spans the period 2000-2011 and was created as part of the effort to build a reference data set for nutrients and dissolved oxygen. The metrics used are RMS of the differences between the observations and the model outputs transformed at the location and time of the observations and correlation. Density plots and vertical profiles are also shown.

Model pH and pCO2 accuracy estimates are based on the results of the comparison between modelled carbonate system variables (i.e. DIC and alkalinity) with an independent dataset gathered from scientific cruises. The metric computed is the RMS difference between a reconstructed climatology and the model outputs averaged to the space resolution of the climatology. The reference dataset considers the period from 1999 to 2013 and includes 4 scientific cruises covering the whole Mediterranean Sea, several scientific cruises in marginal seas and local areas, and a single fixed station (DYFAMED) continuously monitored for several years. Usually, the scientific cruises were conducted during one month mostly in spring or autumn. Data have sparse and scarce spatial and temporal coverage (Table III.3, and Figure III.3), they do not resolve the annual cycle and barely work out the basin wide gradients. The most observed variables are DIC and alkalinity (up to 90% of the samplings), while pH was collected only in less than 30% of the samplings. Therefore, the data have been used to compute two reference climatology datasets for DIC and alkalinity:

- mean maps computed on an 1°x1° grid for selected layers (0-50, 50-100, 50-150, 150-200, 200-500, 500-1000, 1000-1500, 1500-4000 metres);
- mean profiles computed over 18 selected areas 4°x4° wide; areas (Figure III.3) have been selected according to the location and abundance of data.

variables	reference dataset	Description
Chlorophyll	OCEANCOLOUR_MED_CHL_L3_REP_OBSERVATIONS_009_073 and OCEANCOLOUR_MED_CHL_L3_NRT_OBSERVATIONS_009_040	Surface chlorophyll comparison between model output and satellite estimates
Chlorophyll	ISPRA dataset	Chlorophyll comparison between model output and insitu measurement along the Italian coasts
Net primary production	Reference values from scientific publications	Net primary production comparison between integrated model output and reference values
Nitrate	OGS-NODC dataset	Nitrate comparison between model output and insitu data
Nitrate	Climatology from World Ocean Atlas 2013 historical dataset	Nitrate comparison between model output and climatology from historical datasets
Phosphate	OGS-NODC dataset	Phosphate comparison between model output and insitu data
Phosphate	Climatology from World Ocean Atlas 2013 historical dataset	Phosphate comparison between model output and climatology from historical datasets
Dissolved oxygen	OGS-NODC dataset	Dissolved oxygen comparison between model output and insitu data
Alkalinity	Climatology from historical datasets	Alkalinity comparison between model output and a climatology from historical datasets
DIC	Climatology from historical datasets	Dissolved inorganic carbon (DIC) comparison between model output and a climatology from historical datasets

Table III.1. List of metrics.

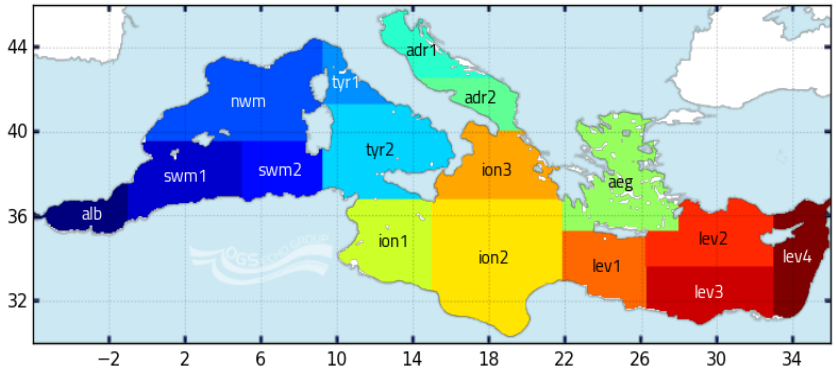

Figure III.1. Subdivision of the model domain in sub-basins used for reanalysis validation. According to data availability and to ensure consistency and robustness of the metrics, different subsets of the sub-basins or some combinations among the given sub-basins can be used for the different metrics.

Nutrients and Dissolved oxygen (from EU/MEDAR/MEDATLAS II and OGS-NODC)		
Dataset name	**Period**	**Area**
SINAPSI 3,4	2002-2003	Eastern Med.
JGOFS-FRANCE	1999	Western Med.
BIOPT 6	2006	Eastern Med.
DYFAMED	1998-2007	North-Western Med.
RHOFI 3,2,1	2001-2003	Ligurian Sea
NORBAL 1, 2, 3, 4	2000-2003	Algerian Sea
CIESM SP1,SP2,SP3	1998-2006	Mediterranean
MELISSA	2004, 2007	Western Med.
MEDGOOS 2, 3, 4, 5	2001-2002	Mediterranean
METEOR 51	2001	Western Med.
REGINA MARIS, GARCIA DEL CID	Apr, Sep 2008	Alboran Sea
SESAME ADRIATIC SEA	Apr, Sep 2008	Adriatic Sea
CARBOGIB 01,02,03,04,05,06	2005-2006	Alboran Sea, Gibraltar Strait
METEOR 84/3	2011	Mediterranean

Table III.2. List of datasets gathered through the OGS-NODC.

Name	Variables	Period	Location	# data	Reference
METEOR51	DIC, ALK, anc. vars	Oct-Nov 2001	TransMed	253	Schneider et al., 2007
BUOM2008	DIC, ALK, anc. vars	June-July 2008	TransMed	567	Touratier et al., 2011
PROSOPE	DIC, pH@25, anc. vars	Sep-Oct 1999	West Med	188	Begovic and Copin, 2013
METEOR 84/3	DIC, ALK, pH@25, anc. vars	Apr 2011	TransMed	845	Tanhua, et al., 2012.
SESAME-EGEO	DIC, ALK, T,S	Apr and Sep 2008	Aegean Sea	265	http://isramar.ocean.org.il/PERSEUS_Data/
SESAME regina_maris	ALK, pH@25, anc. vars	Apr 2008	Alboran Sea	254	http://isramar.ocean.org.il/PERSEUS_Data/
SESAME Garcia del Cid	ALK, pH@25, anc. vars	Sep 2008	Alboran Sea	331	http://isramar.ocean.org.il/PERSEUS_Data/
SESAME Adriatic	ALK, pH@25, anc. vars	Apr and Sep 2008	Adriatic Sea	333	http://isramar.ocean.org.il/PERSEUS_Data/
CARBOGIB	ALK, DIC, pH@25, anc. vars	May, Sept, Dec 2005; Mar, May, Dec 2006	Alboran Sea	229	Huertas, 2007a
GIFT	ALK, DIC, pH@25, anc. vars	Jun, Nov 2005	Alboran Sea	30	Huertas, 2007b
DYFAMED Station	ALK, DIC	Almost monthly from 1999 to 2004	North West Med	707	Copin-Montegut and Begovic, 2002
MEDSEA 2013	DIC, ALK, T,S	May 2013	TransMed	462	Goyet et al., 2015

Table III.3. List of datasets used to build climatology of the carbonate system variables. “TransMed”: scientific cruise that covered the Mediterranean Sea from the Western sub-basin to the Eastern sub-basin; “anc. vars”: ancillary variables (T, S); “pH@25”: pH reported at 25°C.

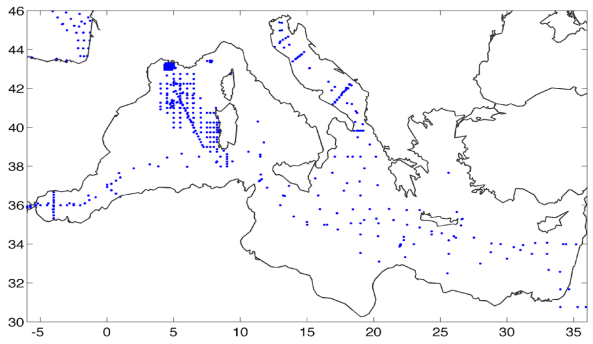

Figure III.2. Map of gathered data of nutrients through the NODC-OGS data set for period 2000-2011.

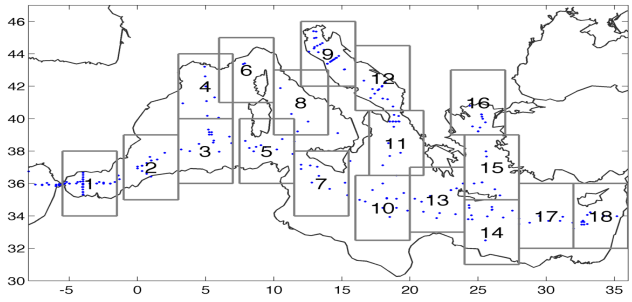

Figure III.3. Location of the carbonate system variables data, and identification of 18 areas 4°x4° wide used for the validation activities.

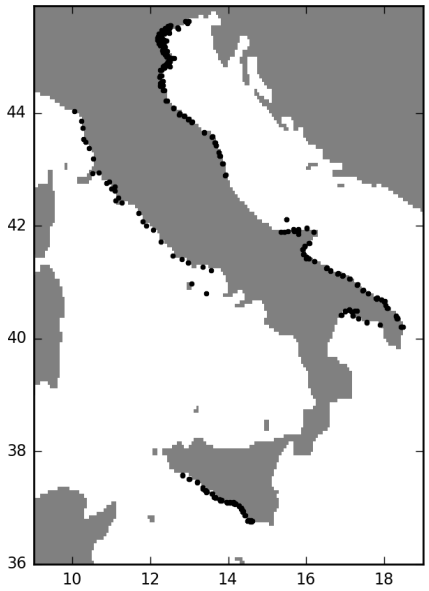

Figure III.4: Location of the coastal monitoring network of ISPRA.

IV VALIDATION RESULTS

IV.1 Chlorophyll

Validation of surface chlorophyll is performed using semi-independent and independent data. In fact, within a cycle of assimilation, re-initialization and simulation, the misfit computed before the assimilation is here used as a measure of the model uncertainty of surface chlorophyll. Indeed, the satellite data are used for assimilation and validation but at different moments. Further, chlorophyll is also assessed in coastal areas using an independent dataset (i.e. monthly in situ measurements of the monitoring network of the Italian National Institute for Environmental Protection and Research, ISPRA).

Averaged annual maps of surface chlorophyll are shown in Figure IV.1. Time series of monthly mean surface chlorophyll concentration for the reanalysis (computed over the sub-surface 10 m layer) and satellite for selected sub-basins and for the Mediterranean Sea are shown in Figure IV.2. As well known, Mediterranean Sea is quite heterogeneous, with sub-basins characterized by different biogeochemical dynamics. The general features, widely described in literature and clearly visible in the maps of Figure IV.1 and in the time series of Figure IV.2, are the higher concentrations and larger seasonal cycles that characterize the western sub-basins with respect to the eastern ones. The results of reanalysis are thus generally consistent with satellite observations. We only observe slight underestimations of the very low summer satellite values for some marginal Seas (ADR1, ADR2), while some of the highest values observed in winter in the Western Mediterranean (SWM1, SWM2 and NWM) are not totally captured by the reanalysis simulation. Focussing on the whole basin-averaged comparison (MED), we can also appreciate the capacity of the reanalysis to reproduce the inter-annual variability (see as an example winters 2001, 2004, 2006, 2009, 2013, 2014 characterized by the highest bloom conditions), and the positive trend over the whole Mediterranean Sea during the investigated period. Validation metrics on open sea are reported in Figure IV.3 and Table IV.1. The new assimilation scheme (i.e. integration of both coastal and open-sea chlorophyll data) provides a good model performance also in the coastal areas (see Tabs. IV.2 and IV.3).

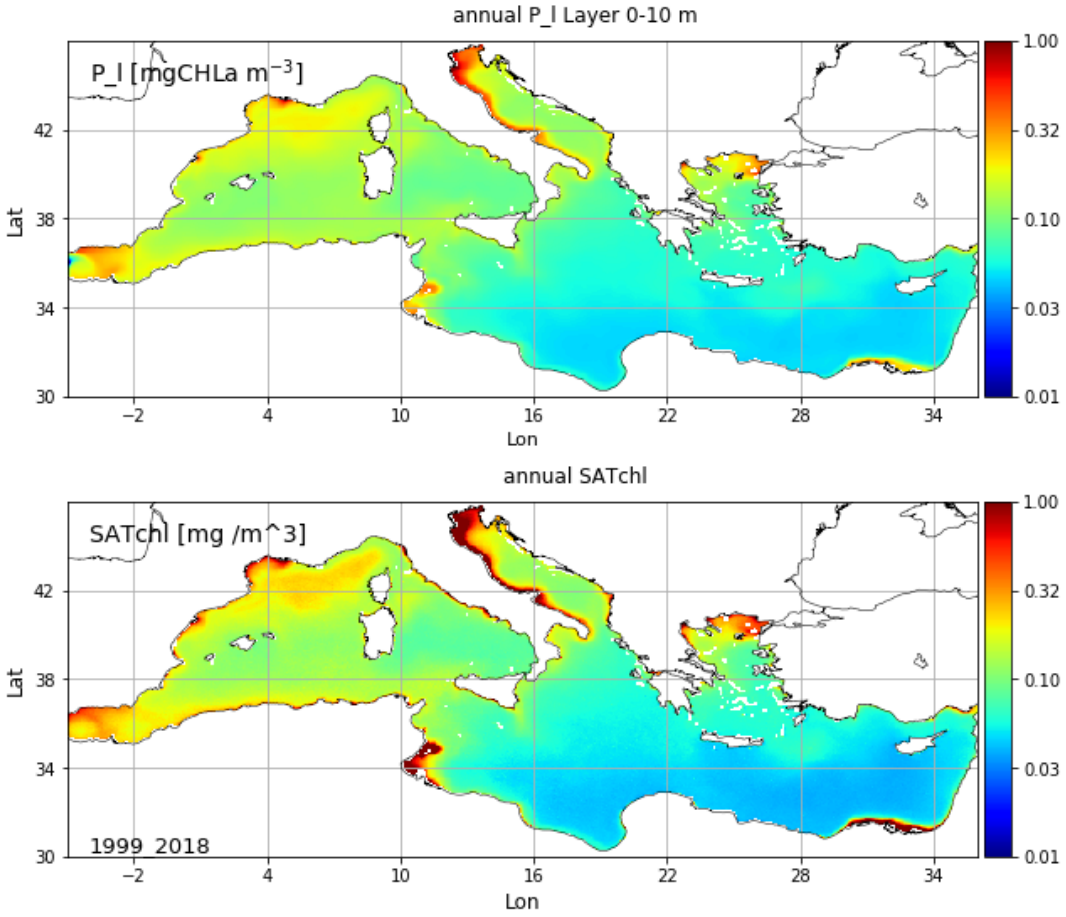

Figure IV.1. Averaged annual maps of surface chlorophyll from reanalysis (left) and from ESA-CCI satellite (right). The average is computed considering the period 1999-2018, and the layer 0-10 m for the model results.

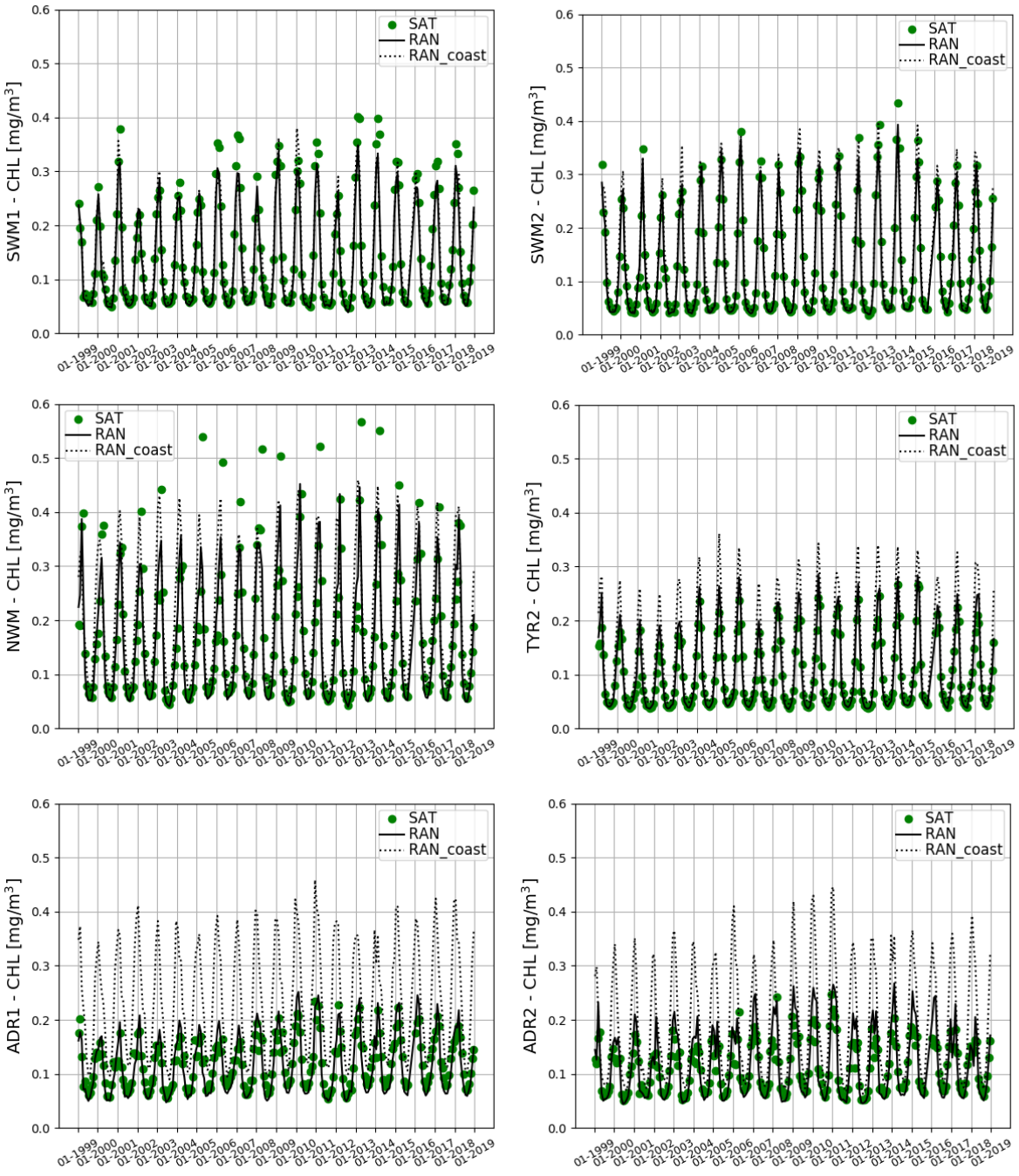

Figure IV.2. 1999-2018 time series of the reanalysis monthly mean surface chlorophyll concentration (black line) compared with ESA-CCI satellite data set (green dots) **for selected sub-basins** and for the Mediterranean Sea (MED). Reanalysis monthly mean surface chlorophyll concentration referred only to coastal areas is also shown (dotted line) (continues overleaf).

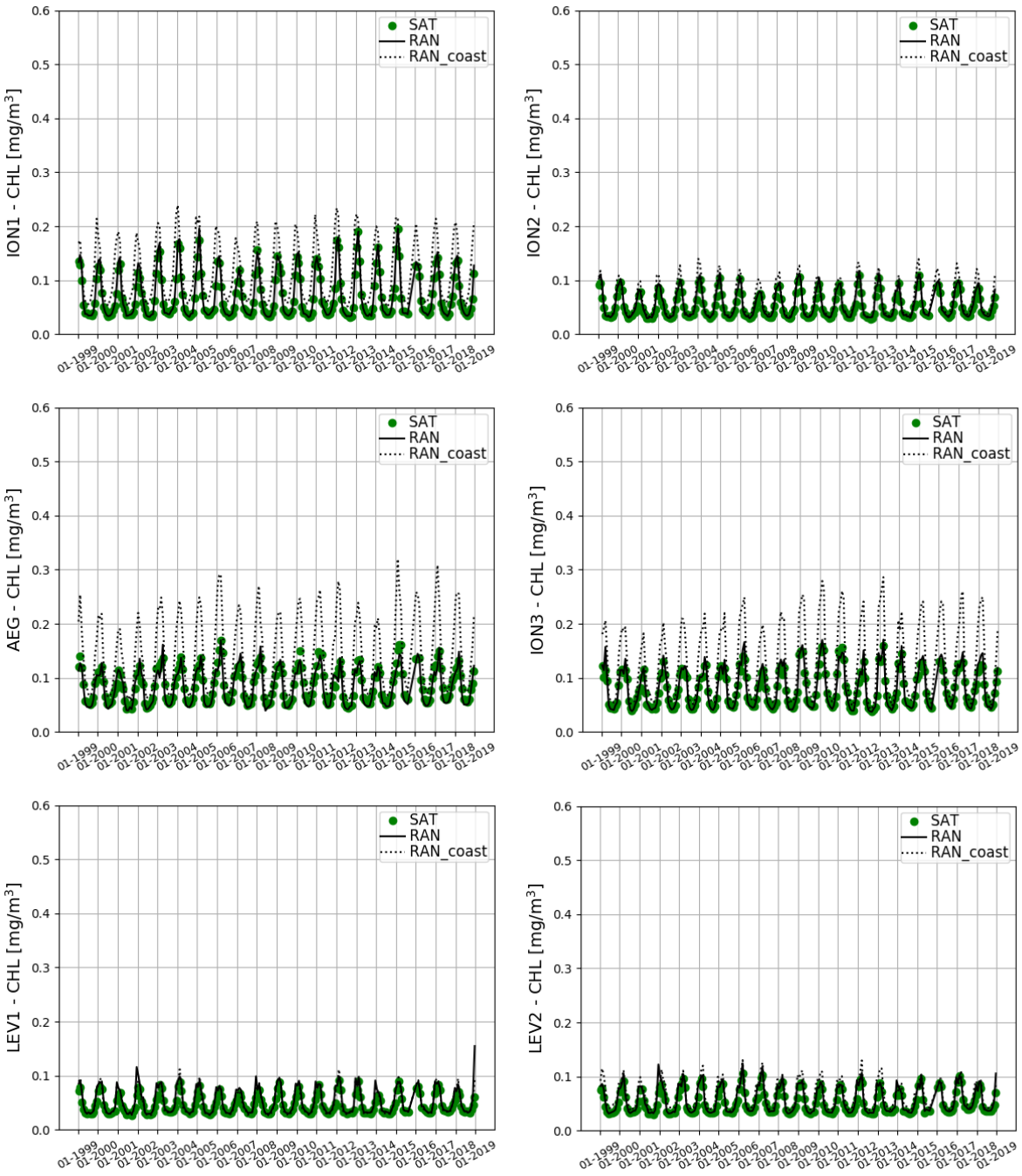

Figure IV.2. (continued) 1999-2018 time series of the reanalysis monthly mean surface chlorophyll concentration (black line) compared with ESA-CCI satellite data set (green dots) **for selected sub-basins** and for the Mediterranean Sea (MED). Reanalysis monthly mean surface chlorophyll concentration referred only to coastal areas is also shown (dotted line) (continues overleaf).

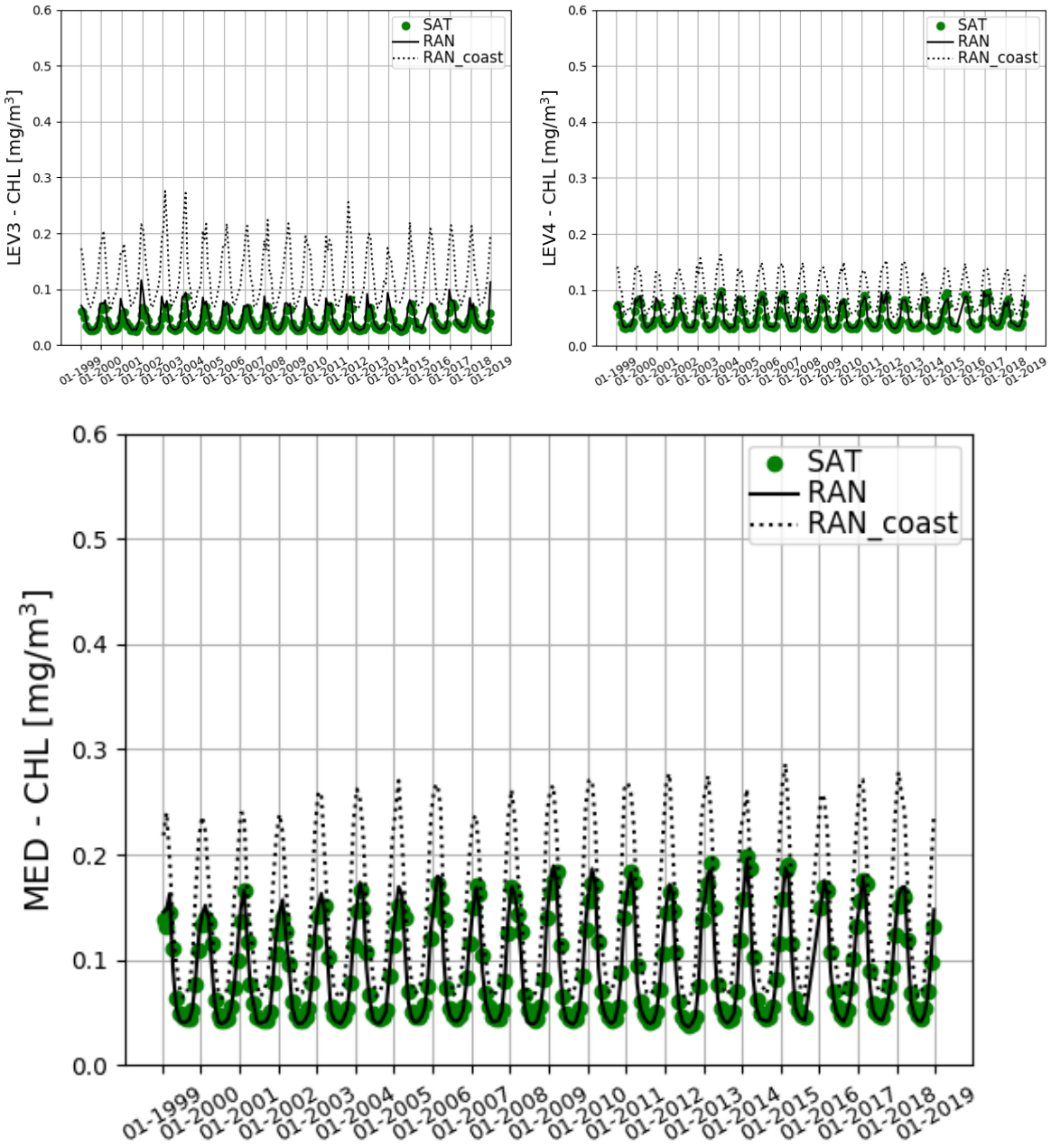

Figure IV.2. (continued) 1999-2018 time series of the reanalysis monthly mean surface chlorophyll concentration (black line) compared with ESA-CCI satellite data set (green dots) **for selected sub-basins** and for the Mediterranean Sea (MED). Reanalysis monthly mean surface chlorophyll concentration referred only to coastal areas is also shown (dotted line).

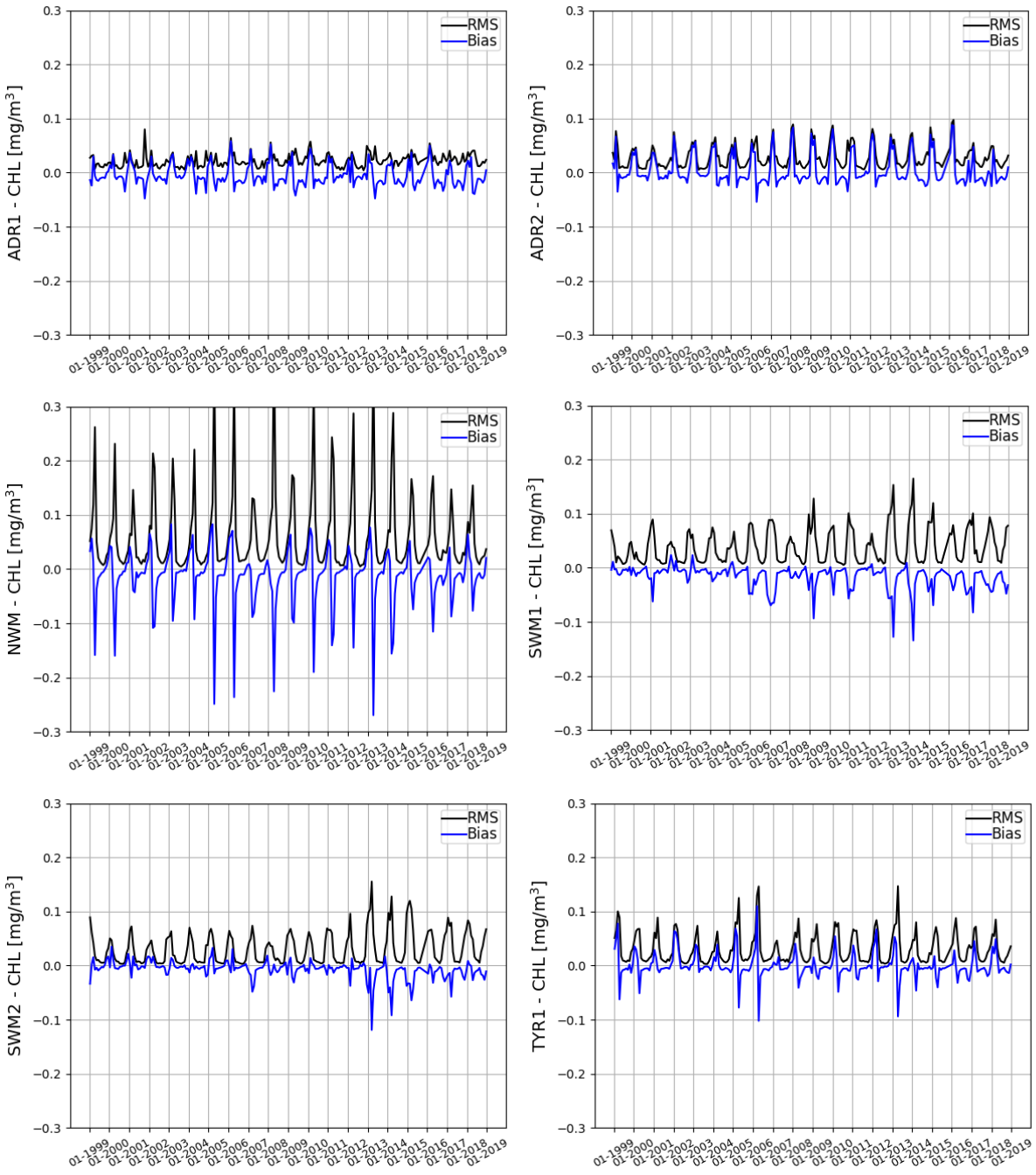

Figure IV.3. 1999-2018 monthly time series of BIAS and RMSD metrics computed for selected Mediterranean sub-basins reported in Figure III.1 and for the Mediterranean Sea (MED). Computation of BIAS and RMSD are based on the reanalysis monthly mean surface chlorophyll concentration referred only to offshore areas (depth deeper than 200 m) (continues overleaf).

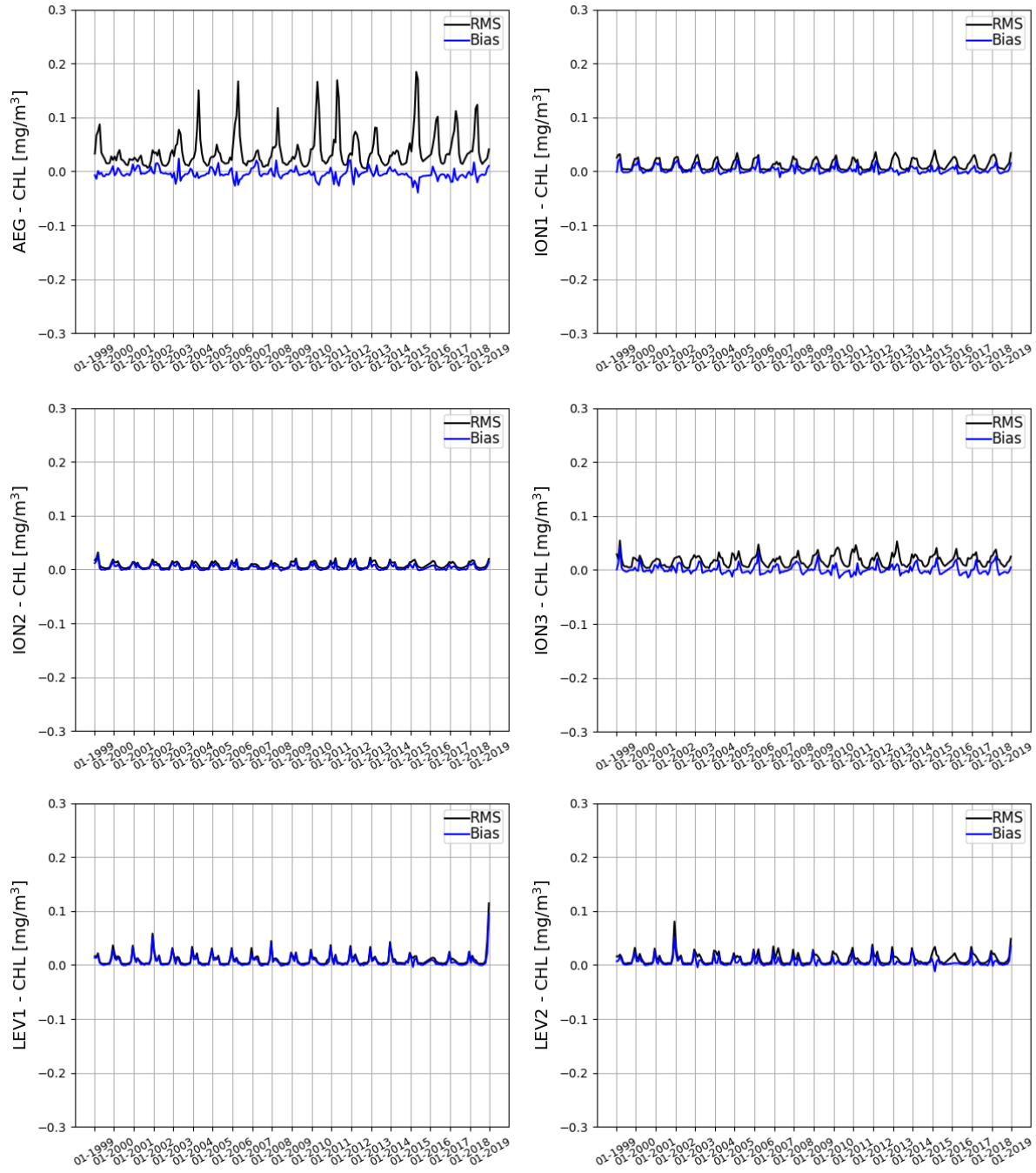

Figure IV.3. (continued) 1999-2018 monthly time series of BIAS and RMSD metrics computed for selected Mediterranean sub-basins reported in Figure III.1 and for the Mediterranean Sea (MED). Computation of BIAS and RMSD are based on the reanalysis monthly mean surface chlorophyll concentration referred only to offshore areas (depth deeper than 200 m) (continues overleaf).

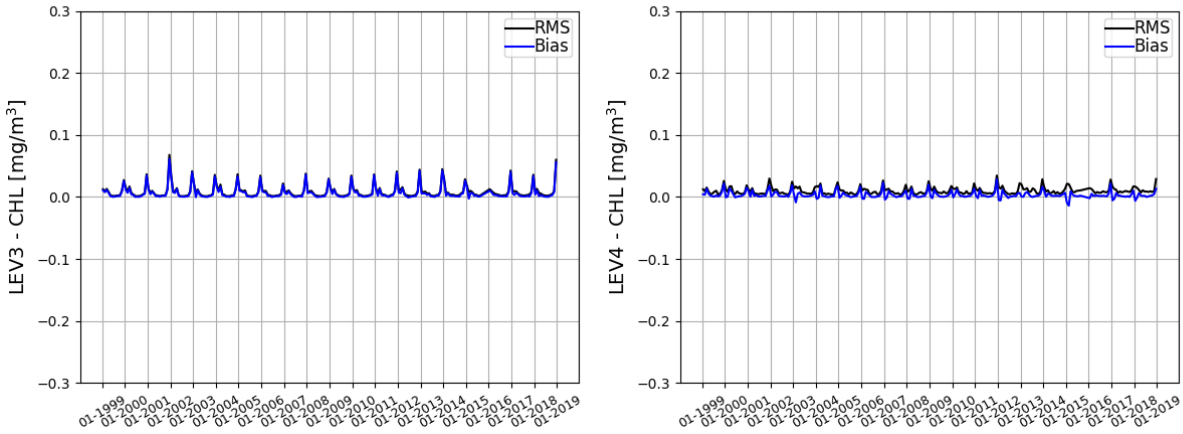

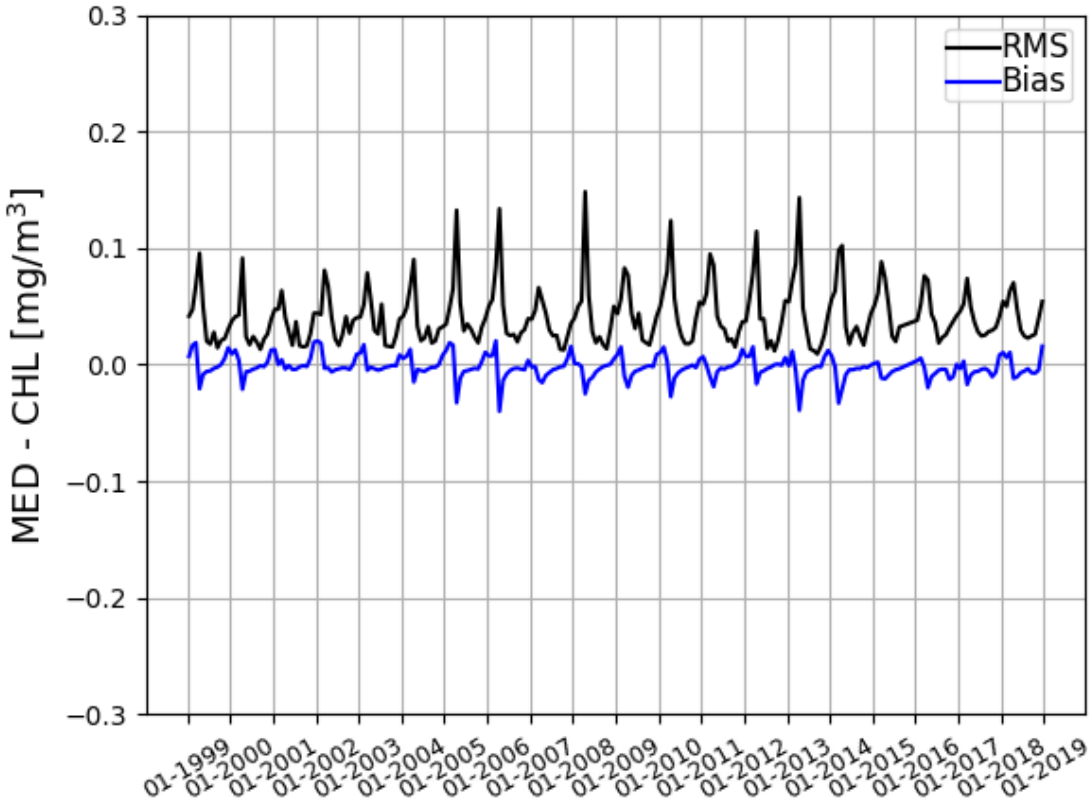

Figure IV.3. (continued) 1999-2018 monthly time series of BIAS and RMSD metrics computed for selected Mediterranean sub-basins reported in Figure III.1 and for the Mediterranean Sea (MED). Computation of BIAS and RMSD are based on the reanalysis monthly mean surface chlorophyll concentration referred only to offshore areas (depth deeper than 200 m).

Metrics (see definition in Table III.1) are computed considering both the natural and the log-transformed chlorophyll. Time series of BIAS and RMS of the differences are plotted in Figure IV.3 for selected sub-basins, and their seasonal averages are reported in Table IV.1. The errors are quite low in all sub-basins and seasons. Observing Figure IV.3, RMSD exceeds 0.1 mg/m^3 only in SWM1, SWM2, NWM and AEG in winter, while ION1/2/3 and LEV1/2/3/4 mainly range lower than 0.05 mg/m^3 during the whole period. Over the whole basin (MED), RMSD exceeds 0.1 mg/m^3 only during few winter months in 2005, 2006, 2008, 2010, 2012 and 2013. The higher values of RMSD in the western sub-basins (NWM in particular) may be also related to a model delay in bloom dynamics of about 3-4 weeks, which is filtered by the monthly averaging. However, in these areas, blooms are strongly related to the presence of local patches, fronts, horizontal circulation structures and local mixing conditions of the water column. A possible source of error for the model forecast might arise from the uncertainty of the physical forcing which can erroneously drive the position of the high-chlorophyll patchiness. The value of the BIAS over the Mediterranean Sea (see Table IV.1), considering the climatological average, is 0.001 and 0.004 mg/m^3 for winter and summer, respectively. Table IV.1 gives also evidence of the model skill with respect to the mean seasonal variability, showing that model accuracy is generally higher in summer in terms of lower RMSD. BIAS appears larger in winter for the western sub-basins and south Adriatic (ALB, SWM1, NWM and ADR2 have absolute winter BIAS larger than 0.02 mg/m^3), possibly related to the intense productive processes strongly coupled with the physical mechanisms, that may not be fully represented in the forcings.

OPEN SEA	Surface (0-10 m) chlorophyll Mod-Sat				Surface (0-10 m) chlorophyll log_{10}(Mod)-log_{10}(Sat)			
	RMSD		BIAS		RMSD		BIAS	
	win	sum	win	sum	win	sum	win	sum
ALB	0.168	0.127	-0.064	-0.035	0.669	0.640	-0.179	-0.156
SWM1	0.062	0.010	-0.025	-0.007	0.100	0.065	-0.038	-0.047
SWM2	0.056	0.006	-0.011	-0.004	0.092	0.050	-0.013	-0.038
NWM	0.134	0.015	-0.023	-0.011	0.157	0.081	0.004	-0.064
TYR1	0.062	0.008	0.010	-0.006	0.109	0.058	0.020	-0.044
TYR2	0.041	0.005	0.015	-0.003	0.098	0.043	0.036	-0.029
ADR1	0.030	0.015	0.013	-0.013	0.079	0.084	0.029	-0.080
ADR2	0.051	0.012	0.033	-0.010	0.133	0.077	0.084	-0.069
AEG	0.057	0.017	-0.003	-0.006	0.095	0.071	0.013	-0.030
ION1	0.021	0.004	0.006	-0.001	0.070	0.039	0.025	-0.009
ION2	0.013	0.003	0.007	0.000	0.066	0.032	0.040	0.003
ION3	0.027	0.007	0.007	-0.003	0.081	0.048	0.035	-0.023
LEV1	0.013	0.003	0.009	0.001	0.081	0.031	0.060	0.007
LEV2	0.016	0.003	0.006	0.001	0.078	0.035	0.039	0.010
LEV3	0.010	0.002	0.008	0.001	0.072	0.029	0.056	0.011
LEV4	0.013	0.006	0.003	0.001	0.070	0.057	0.027	0.015
MED	0.067	0.024	-0.001	-0.004	0.152	0.122	0.020	-0.023

Table IV.1. Mean RMSD and BIAS between surface chlorophyll model maps and satellite maps referred to open sea areas (depth larger than 200 m). On the right side, the skill indexes are computed on the

model and satellite chlorophyll log-transformed. Winter (win) corresponds to January to April, summer (sum) corresponds to June to September.

The upgrade of the 3DVAR-BIO data assimilation scheme, that now includes the assimilation of satellite chlorophyll over the full domain, produced a good agreement of the surface chlorophyll patterns also in the coastal area (Figure IV.1), and an improvement of the chlorophyll product quality in the coastal areas with respect to the previous reanalysis V2 version (decreases of 22% of BIAS and 17% of RMSD computed on the ISPRA independent dataset[1]).

Tables IV.2 and IV.3 report the skill assessment using both semi-independent and independent data for the coastal areas. In particular, Table IV.2 reports the averages of the times series of RMSD and BIAS computed on the misfit over the coastal area of the sub-basins of Figure III.1, while Table IV.3 reports the Class 4 metrics computed using the monthly in-situ measurements of the ISPRA Italian coastal monitoring network for the five sub-basins that encompass the Italian coasts.

In the coastal areas, the model nearly always underestimates the satellite values (negative BIAS in Table IV.2). RMSD values (Table IV.2) are higher in winter than in summer, and are higher than 0.5 mg/m^3 only in ADR1, ION1 and LEV3 where very high values of chlorophyll are also related to important rivers and continental shelf dynamics (Po river, Gulf of Gabes, Nile river, respectively).

Table IV.3 shows that, in general, model underestimates in-situ coastal observations (higher underestimation in winter-spring). BIAS and RMSD values computed on the in-situ data are much higher than those of Table IV.2 because the available in-situ observations are very close to the coast (less than 4.5 km from the shore, i.e. 1 model gridpoint) and may be characterized by very high values (even much higher than 20 mg/m^3) which can be hardly reproduced by the present configuration of the model. Among the sub-basins, the uncertainty (RMSD) is always lower than 1 mg/m^3 but ADR1. ADR1 statistics are influenced by the sampling stations located in the Po river mouth area, which is by far the most eutrophic area of the Mediterranean Sea.

[1] Metrics of Table IV.3 have been computed on both V4 and V2 reanalysis (data for V2 not shown). The improvement of V4 is estimated by computing the averages of the difference between the V4 and V2 reanalysis BIAS and RMSD.

COAST	Surface (0-10 m) chlorophyll Mod-Sat				Surface (0-10 m) chlorophyll log_{10}(Mod)-log_{10}(Sat)			
	RMSD		BIAS		RMSD		BIAS	
	win	sum	win	sum	Win	sum	win	sum
ALB	0.383	0.265	-0.172	-0.101	0.928	0.627	-0.297	-0.230
SWM1	0.165	0.051	-0.067	-0.021	0.169	0.143	-0.078	-0.095
SWM2	0.442	0.145	-0.132	-0.023	0.242	0.168	-0.080	-0.077
NWM	0.285	0.099	-0.124	-0.043	0.204	0.176	-0.092	-0.122
TYR1	0.373	0.115	-0.142	-0.036	0.247	0.227	-0.107	-0.128
TYR2	0.284	0.120	-0.071	-0.027	0.195	0.173	-0.048	-0.095
ADR1	0.846	0.760	-0.285	-0.263	0.219	0.324	-0.107	-0.224
ADR2	0.439	0.178	-0.175	-0.075	0.224	0.231	-0.094	-0.165
AEG	0.434	0.148	-0.110	-0.037	0.189	0.159	-0.044	-0.098
ION1	0.698	1.779	-0.170	-0.399	0.252	0.400	-0.105	-0.177
ION2	0.050	0.054	-0.005	-0.010	0.116	0.155	0.002	-0.042
ION3	0.183	0.077	-0.043	-0.030	0.182	0.192	-0.038	-0.122
LEV1	0.020	0.024	0.008	-0.003	0.097	0.102	0.054	-0.011
LEV2	0.107	0.036	-0.048	-0.017	0.214	0.192	-0.102	-0.104
LEV3	0.946	0.654	-0.464	-0.270	0.414	0.434	-0.223	-0.240
LEV4	0.481	0.427	-0.176	-0.150	0.338	0.410	-0.176	-0.235
MED	0.577	0.860	-0.159	-0.155	0.257	0.294	-0.090	-0.148

Table IV.2. Mean RMSD and BIAS between surface chlorophyll model maps and satellite maps referred to coastal areas. On the right side, the skill indexes are computed on the model and satellite chlorophyll log-transformed. Winter (win) corresponds to January to April, summer (sum) corresponds to June to September.

	RMSD		BIAS		n. of measurements	
	win	sum	win	sum	win	sum
ADR1	1.73	1.11	-1.00	-0.64	967	1204
ADR2	0.40	0.36	0.02	0.02	169	158
ION3	0.16	0.10	<0.01	-0.07	38	43
TYR1	0.27	0.48	0.07	-0.31	51	66
TYR2	0.26	0.09	-0.20	-0.07	82	77

Table IV.3. RMSD and BIAS between surface chlorophyll model and in-situ measurements of the ISPRA dataset for the Italian coastal areas. Given the normal distribution of the chlorophyll concentrations of the data set, the skill indexes are computed on the model and in situ non-log-transformed chlorophyll. Winter (win) corresponds to January to June, summer (sum) corresponds to July to December.

IV.2 Net primary production

Net primary production (NPP) is the measure of the net uptake of carbon by phytoplankton groups (gross primary production minus fast release processes – e.g. respiration). The lack of any extensive dataset of measures of primary production prevents the application of quantitative metrics for the assessment of the quality of this product. Thus, the product quality consists in a qualitative assessment of the consistency of the modelled NPP with previous estimates published in scientific literature (Figures IV.4 and 5 and Table IV.4). Relevant gradients between eastern and western regions and averaged estimates reanalysis in the different sub-basins of the reanalysis are consistent with basin-wide estimates (maps from Lazzari et al., 2012) and with sub-basin averages (Table IV.4). The reanalysis depicts a slight overestimation in the eastern Mediterranean sub-basin. The climatological monthly values computed from the reanalysis (Figure IV.5) are in any case consistent with the range of variability given by short period estimates reported by Siokou-Frangou et al. (2010; see Table IV.4).

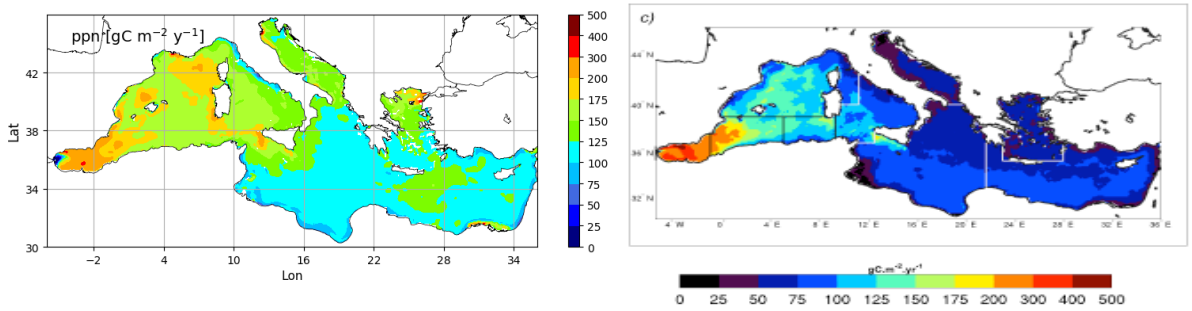

Figure IV.4. Annual averaged vertically integrated primary production (gC m^{-2} yr^{-1}) from reanalysis (left) and from reference multi-annual simulation (Lazzari et al., 2012; right).

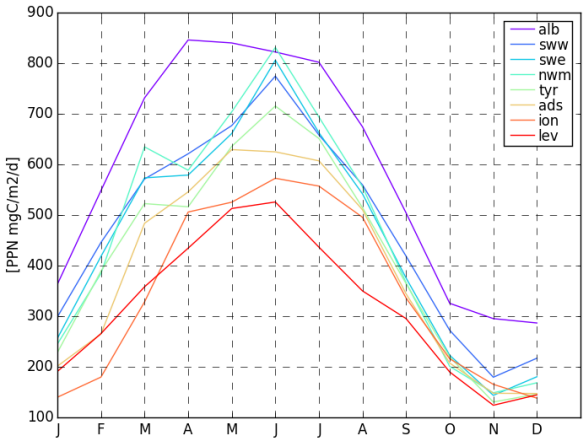

Figure IV.5. Monthly climatology of vertically integrated primary production (mgC m^{-2} d^{-1}) computed from the reanalysis in the open sea areas.

	Lazzari et al. (2012)	Colella (2006); Satellite estimates	Siokou-Frangou et al., 2010 (Reported in Table 1, only in-situ estimates)		CMEMS Reanalysis: 1999-2016
	Annual mean [gC/m^2/y]	Annual mean [gC/m^2/y]	Annual mean [gC/m^2/y]	Short term estimates [mgC/m^3/d]	Annual mean [gC/m^2/y]
Mediterranean Sea (MED)	98±82	90±48			136±33
Alboran Sea (ALB)	274±155	179±116		353–996; May-Jun1996 142; Nov2003	214±63
South West Med -West (SWM1)	160±89	113±43		186–636 (avg. 440) Oct1996	174±13
South West Med -East (SWM2)	118±70	102±38			166±13
North West Med (NWM)	116±79	115±67	105.8-119.6 86-232 (only DYFAMED station) 140-170 (South Gulf of Lion)	353–996; May–Jun1996 401; Mar-Apr1998 (G. Lion) 166; Jan-Feb1999 (G. Lion) 160–760; May-Jul (Cat-Bal) 150–900; Apr1991 (Cat-Bal) 450, 700; Jun1993 (Cat-Bal) 210, 250; Oct1992 (Cat-Bal) 1000±71 Mar1999 (Cat-Bal) 404±248 Jan-Feb00 (Cat-Bal)	164±27
Levantine (LEV1+LEV2+LEV3+LEV4)	76±61	72±21	59 (Cretan Sea)		117±14
Ionian Sea (ION1+ION2+ION3)	77±58	79±23	61.8	119–419; May-June 1996 208–324; April-May 1999 186±65; August 1997-98	115±16
Tyrrhenian Sea (TYR1 + TYR2)	92±5	90±35		398; May–Jun1996 273; Jul2005 429; Dec2005	152±17

Table IV.4. Annual averages and short period estimates of the vertically integrated primary production for some selected sub-regions. Estimates are from multi-annual simulation (Lazzari et al., 2012), from satellite model (Colella, 2006), from in-situ estimates (Siokou-Frangou et al., 2010) and from CMEMS system reanalysis.

IV.3 Phosphate and Nitrate

The assessment of the quality of the reanalysis in reproducing basin-wide gradients of nutrients is performed on a qualitatively basis by comparing the modelled maps of nutrients with the basin-wide reconstruction obtained from the World Ocean Atlas 2013 database (1 degree resolution) at different vertical layers (Figure IV.6a and b). Relevant gradients between western and eastern sub-basins and between the surface and the sub-surface layers are well reproduced by the present reanalysis product. In general, reanalysis shows for phosphate lower values in the surface layers (down to 60 m) with respect to WOA2013, in particular in the Northern Western Mediterranean, in the Aegean Sea and in the Levantine basin in the area between Turkey and Cyprus. Below 60 m reanalysis appears to be in good agreement with WOA. Reanalysis nitrate maps appear more in agreement with WOA2013 also in the surface layers.

It is worth to note that biases between reanalysis products and WOA2013 in the upper layers are also related to the low reliability of WOA surface values. In fact, WOA2013 reconstruction shows extreme scattered maps and values of standard deviation even higher than the mean for many bins. This is due to the very low number of observations (on average less than 5 in a single $1^{o}x1^{o}$ bin, with only the Gulf of Lions being the richest area with a number of observations higher than 25).

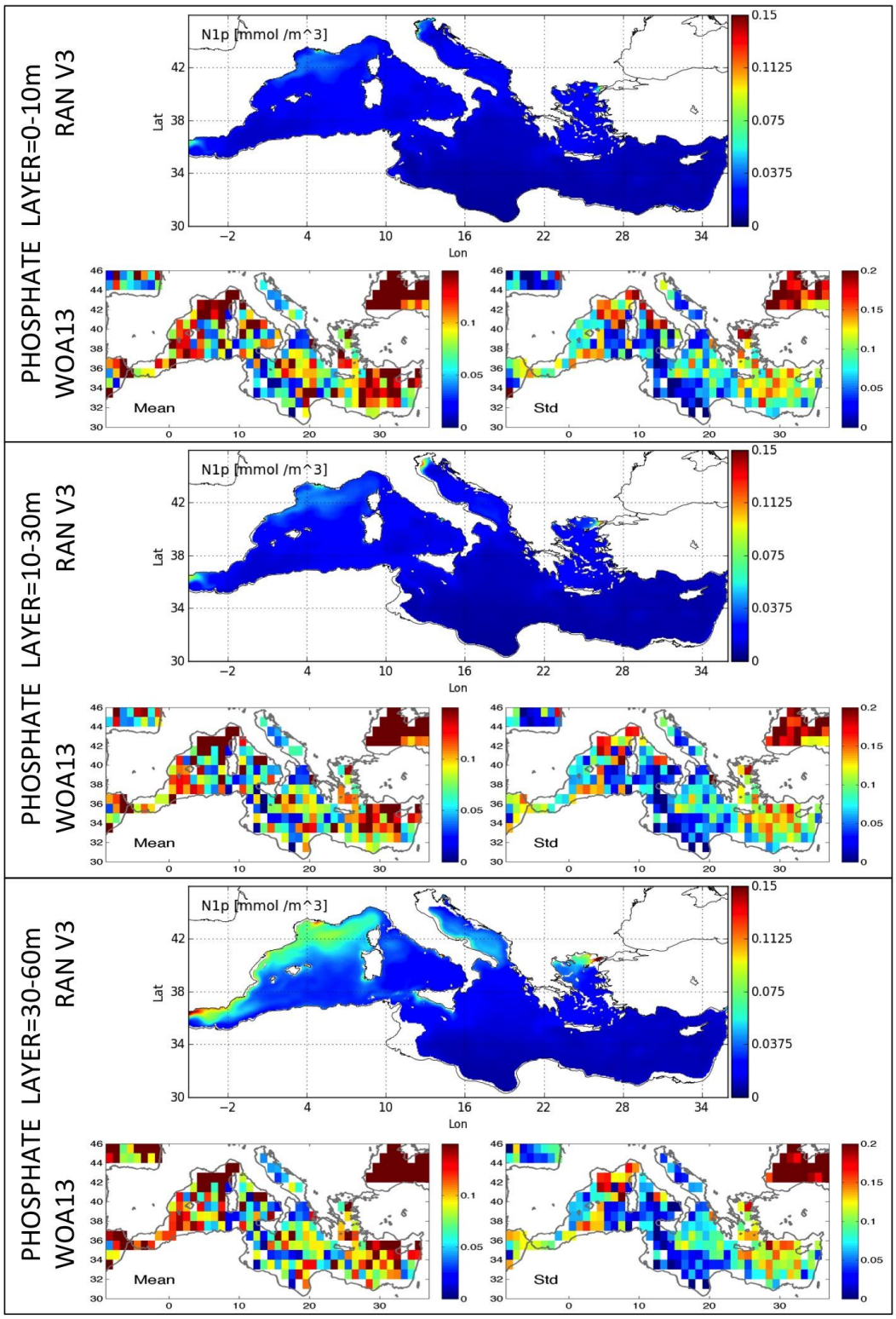

Figure IV.6a. Phosphate ("N1p", mmol P/m^3) mean spatial distributions. Annual average and vertical average over the 0-10, 10-30, 30-60, 60-100, 100-150 and 150-300 m layers from reanalysis (RAN, top in each panel) and from WOA2013 (mean and standard deviation, bottom in each panel) (continues overleaf).

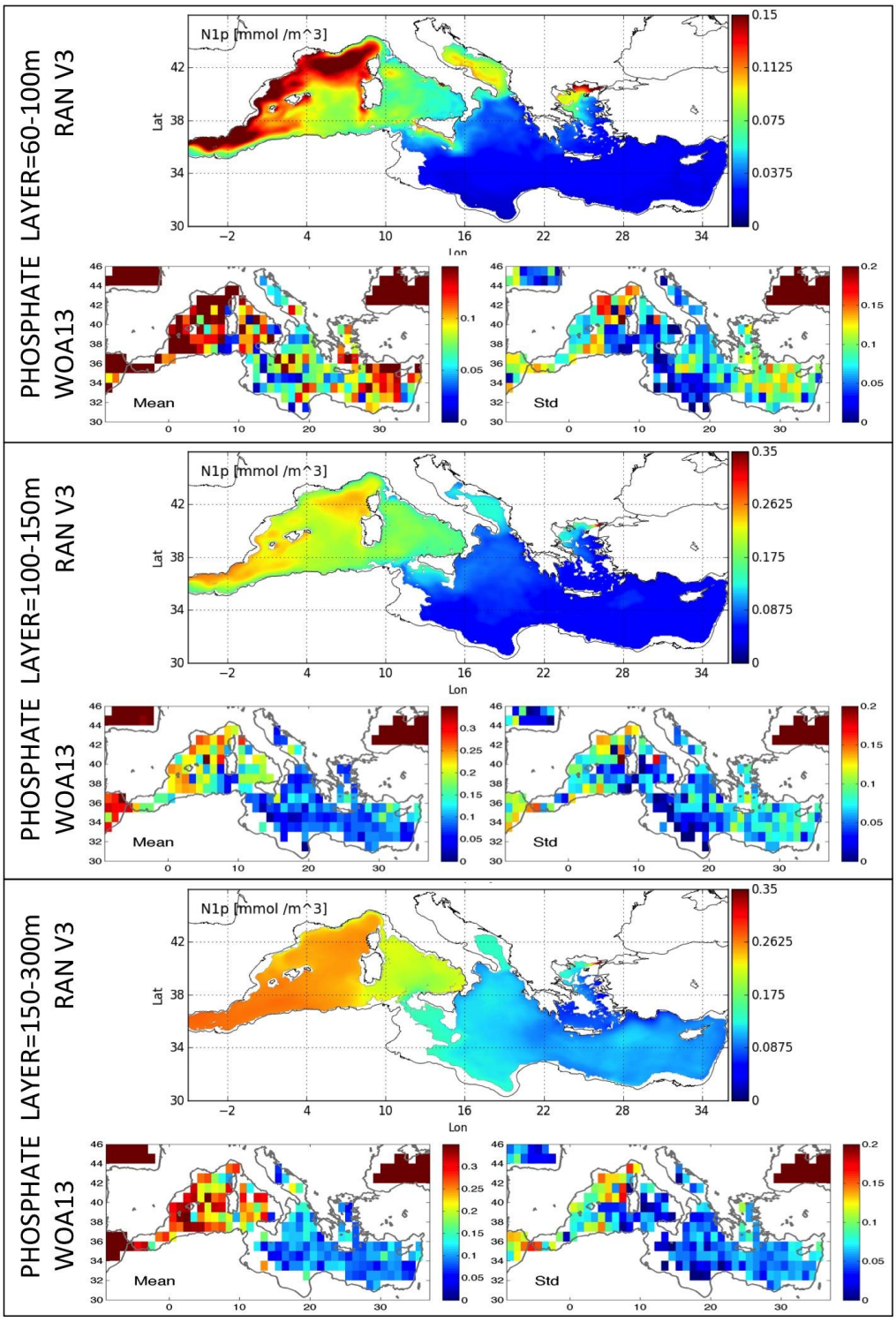

Figure IV.6a. (continued) Phosphate ("N1p", mmol P/m^3) mean spatial distributions. Annual average and vertical average over the 0-10, 10-30, 30-60, 60-100, 100-150 and 150-300 m layers from reanalysis (RAN, top in each panel) and from WOA2013 (mean and standard deviation, bottom in each panel).

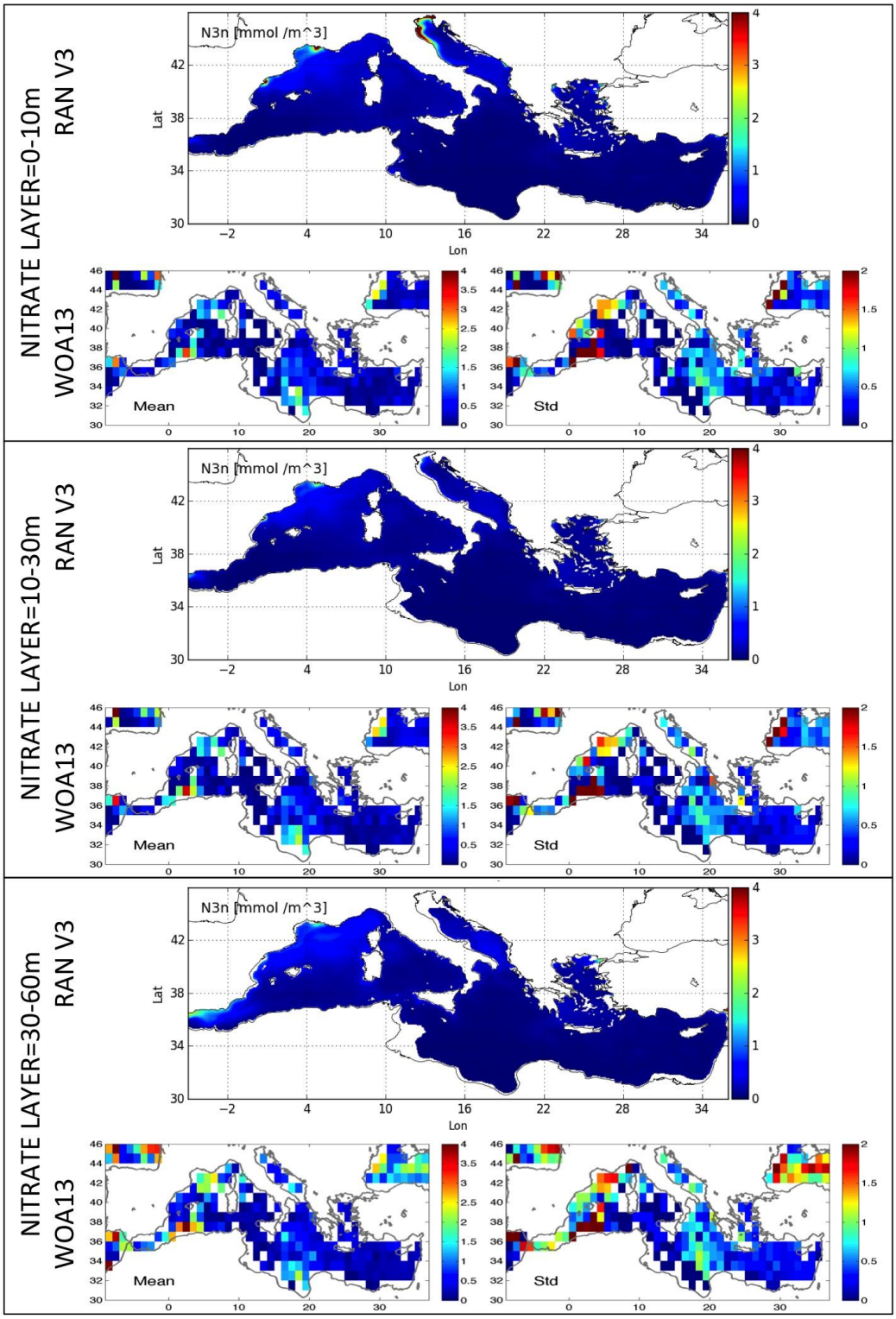

Figure IV.6b. Nitrate ("N3n", mmol N/m^3) mean spatial distributions. Annual average and vertical average over the 0-10, 10-30, 30-60, 60-100, 100-150 and 150-300 m layers from reanalysis (RAN, top in each panel) and from WOA2013 (mean and standard deviation, bottom in each panel) (continues overleaf).

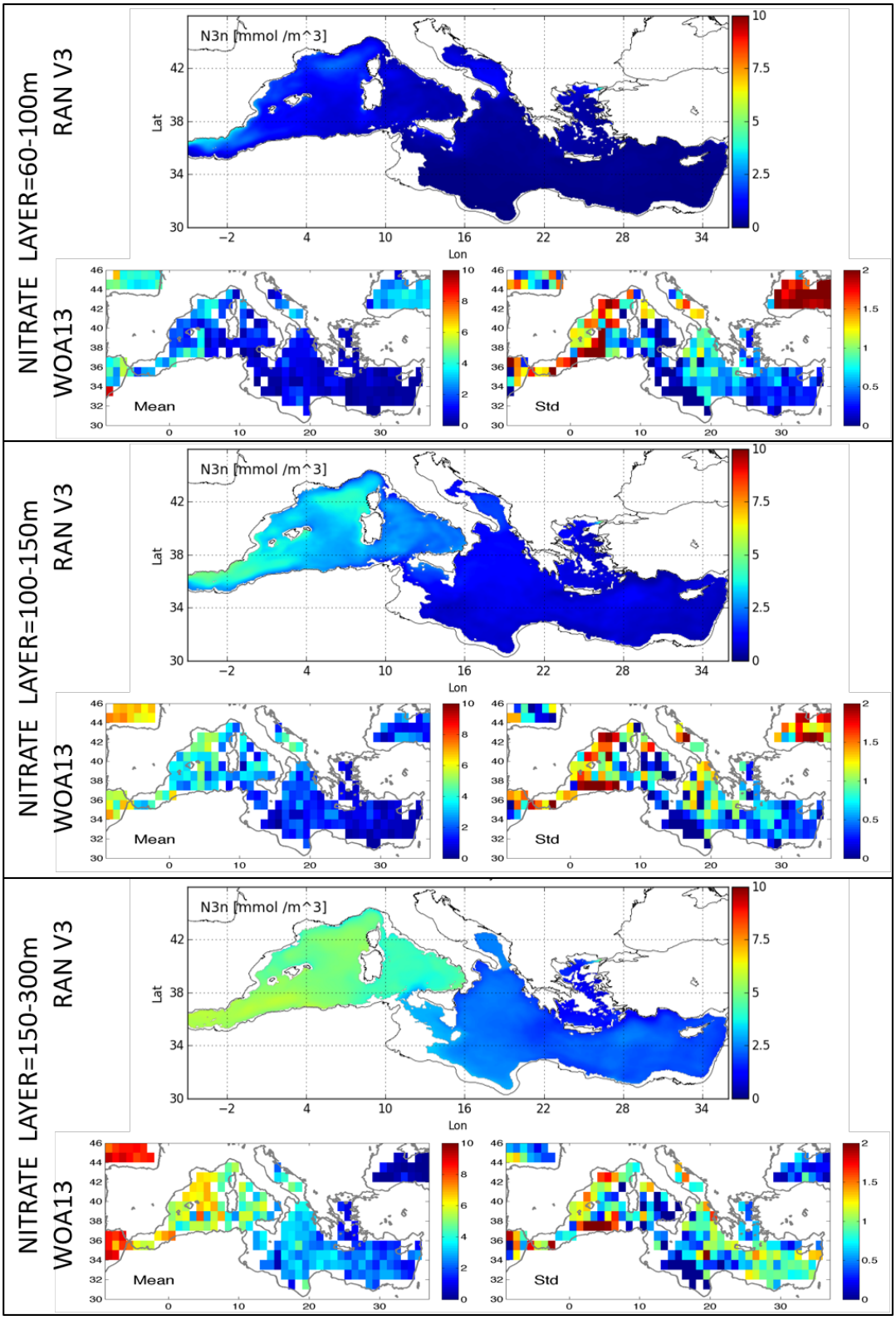

Figure IV.6b. (continued) Nitrate ("N3n", mmol N/m^3) mean spatial distributions. Annual average and vertical average over the 0-10, 10-30, 30-60, 60-100, 100-150 and 150-300 m layers from reanalysis (RAN, top in each panel) and from WOA2013 (mean and standard deviation, bottom in each panel).

In the following figures and tables, the reanalysis outputs are validated against the in-situ dataset that was specifically gathered for this activity through the OGS-NODC. The largest number of model-observation matchups is for phosphate data (8190), while nitrate has 4566 available observations. In particular, for phosphate, NWM has one order of magnitude of matchups (5766) more than LEV (670). It is worth to remind that the comparison using metrics based on model-observation matchups is quite conservative, since the in-situ observations have a scarce coverage of the basin-wide processes but are largely influenced by local and short-term processes.

The RMSD metric for phosphate (definition in Table III.1) is reported for each sub-basin and for different layers, which are consistent with the depth subdivision of the physical reanalysis validation assessment. Since the comparison involves the whole period of simulation, and due to the scarcity of the reference data set, the RMSD here proposed may give to users some indications on the quality of the products but cannot be considered as a full qualification of the reanalysis product. In fact, it is worth to remind that the variability of reanalysis output is lower than that of observations, since the temporal discretization of model output (monthly means) is different than observations (basically derived by research cruises of few weeks in a specific period of the year). Therefore, model tends to filter out the extreme values that can be captured during a short-term field experiment, thus possibly originating larger differences with observation data.

In terms of phosphate at the surface layer (0-10 m), Table IV.5 shows that RMSD ranges from 0.01 mmol P/m^3 in AEG and LEV to 0.10 mmol P/m^3 in NWM, and that the averaged accuracy over the whole basin 0.03 mmol P/m^3. In general, western sub-basins present higher RMSD than eastern sub-basins. Higher values of phosphate in the Western Mediterranean (see Figure IV.6a at surface and sub-surface layers) and complex biogeochemical dynamics that characterize the western sub-basins (see in particular ALB, SWM1, SWM2 and NWM in comparison to ION and LEV) are the main causes of the larger uncertainty of modelled values in the western sub-basins. Considering all the layers, we observe that the RMSD in western sub-basins mainly exceeds 0.10 mmol P/m^3 in ALB, SWM1, SWM2 and NWM below 100 m (with maximum 0.21 mmol P/m^3 in SWM2 in the layer 300-600 m), possibly related to the different position of the nutricline between the observations and the model. RMSD in eastern sub-basin is generally lower than 0.09 mmol P/m^3, with maxima in the 150-300 m and 600-1000 m layers.

The previous considerations on RMSD are complemented with the analysis of the density plots for some sub-basins (FigureIV.7). The general picture is that model variability is much lower than reference variability: this is quite obvious since 1) the observations can be very localized in time and space, 2) the reanalysis outputs are monthly averaged, thus filtering out the extreme values. The vertical profiles plotted in Figure IV.8 confirm, from a visual point of view, the previous considerations: the MedBFM1 model system reproduces well the main differences between the sub-basins and the vertical structure of the phosphate distributions (see also overall correlation indexes Table IV.5, on average at 0.83) but the model exhibits smaller temporal and spatial variability compared to observations due to the monthly resolution of the reanalysis product. Finally, Figure IV.8 shows that the underestimation of NWM might be also due to an error in initialization of the deepest part (< 2000 m) of the water column.

	RMSD							CORR.	n. of profiles/matchups
	0-10	10-50	50-100	100-150	150-300	300-600	600-1000		
ALB	0.04	0.04	0.10	0.13	0.11	0.16	0.18	0.89	6/72
SWM1	0.02	0.02	0.11	0.09	0.10	0.13	0.13	0.84	7/108
SWM2	0.06	0.10	0.10	0.10	0.14	0.21	0.16	0.82	44/347
NWM	0.10	0.09	0.13	0.13	0.14	0.15	0.13	0.84	535/5766
TYR	0.02	0.03	0.06	0.05	0.07	0.08	0.06	0.88	12/143
ADN	-	-	-	-	-	-	-	-	0/0
ADS	0.04	0.03	0.04	0.04	0.05	0.04	0.04	0.67	21/217
AEG	0.01	0.01	0.02	0.05	0.06	0.04	0.03	0.68	5/56
ION	0.03	0.03	0.03	0.03	0.09	0.06	0.09	0.70	46/811
LEV	0.01	0.01	0.03	0.05	0.08	0.08	0.08	0.67	50/670
MED	0.03	0.02	0.03	0.04	0.08	0.07	0.09	0.83	726/8190

Table IV.5. Mean RMSD between phosphate model outputs and NODC-OGS dataset computed at the in situ observation locations. The metric is calculated for selected layers (0-10 m, 10-50 m, 50-100 m, 100-150 m, 150-300 m, 300-600 m, 600-1000 m), and averaged over the whole reanalysis period. Sub-basins are those of Figure III.1 or combinations of them (i.e. TYR=TYR1+TYR2; ION=ION1+ION2+ION3; LEV=LEV1+LEV2+LEV3+LEV4). The overall correlation between observations and model output is also reported with references of n. of profiles and matchups available.

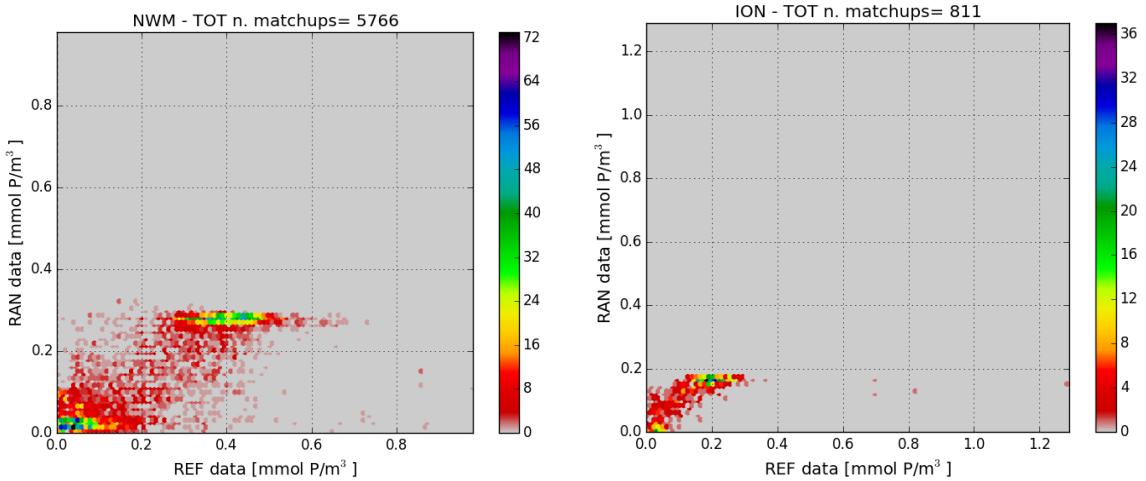

Figure IV.7. Density plots for model (RAN, y-axis) and reference (REF, x-axis) matchups of phosphate (mmol P/m^3) for ALB, NWM, ION and LEV.

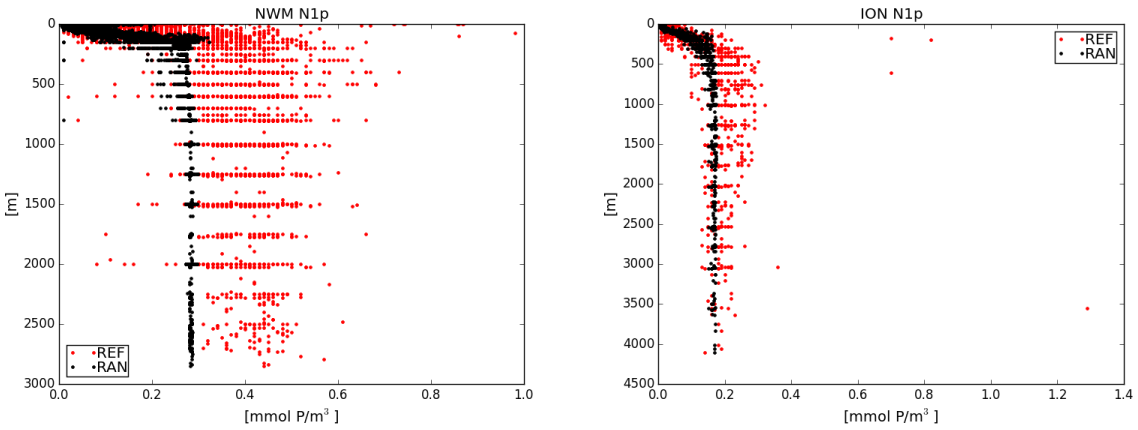

Figure IV.8. Vertical profiles of phosphate (mmol P/m^3) for reanalysis (RAN) and reference dataset (REF) for some selected sub-basins.

The implementation of the skill assessment for nitrate is reported in Table IV.6 (RMSD metric defined in Table III.1 and overall correlation) and in Figures IV.9 (density plots) and IV.10 (vertical profiles). Results of the comparison indicate that the comments referred to phosphate are, in general, valid also for RMSD metrics computed for nitrate (Table IV.6): the western sub-basins present the largest errors. The largest RMSD is computed for NWM at surface layer (3.52 mmol P/m^3, almost one order of magnitude larger than the Mediterranean average RMSD at surface layer), while all the other sub-basins present errors at surface not exceeding 0.64 mmol N/m^3 in the western (ALB) and 0.50 mmol N/m^3 in the eastern (ION and LEV). Most of sub-basins have the largest error in the intermediate and deep layers, with a maximum in the 300-600 m layer of 4.44 mmol N/m^3 in SWE and never exceeding 2 mmol N/m^3 in the eastern sub-basins. These are the most critical layers, because small errors in the displacement of the nutricline may produce large quantitative errors. Indeed, inconsistency in vertical displacements might arise also from the model vertical discretization that is 10 m at the depth of 100 m, growing to 36 m at 500 m. However, it is worth to note that the shapes of the vertical profiles are quite well reproduced by the reanalysis (correlation higher than 0.80 in most of the sub-basins and mean correlation on the whole basin of 0.68, Table IV.6).

The considerations on RMSD are complemented with the analysis of the density plots for some sub-basins (Figure IV.9). The largest errors are due to the lower variability of modelled data with respect to observations. In the density plots, several clouds of points can have a very compressed and horizontal elongated shape, which means that the reanalysis monthly output does not reproduce the variability related to small-scale spatial and temporal features observed in in-situ data.

The general picture showed in Figure IV.10 gives evidence that the accuracy of reanalysis is quite good in reproducing the differences among sub-basins (different mean values at the deep layers) and the mean vertical structures of the nitrate (lower values at surface, a nutricline between 100 and 500 m, and a constant profile in the deepest part). The general underestimation of sub-surface values (between 100 and 600 m) shown in Figure IV.10, in particular for NWM, is the cause of the bad performance of RMSD metrics. It is worth to remind that most observations in NWM are related to one single point (DYFAMED station), thus a not well resolved local dynamics might increase the bias for the results of the sub-basin analysis.

	RMSD							CORR.	n. of profiles/matchups
	0-10	10-50	50-100	100-150	150-300	300-600	600-1000		
ALB	0.64	1.11	2.86	3.11	2.92	4.24	3.66	0.88	6/66
SWW	0.55	0.60	2.24	1.99	2.58	2.94	2.65	0.90	7/114
SWE	0.62	1.80	2.28	3.01	3.24	4.44	2.86	0.65	47/333
NWM	3.52	2.26	3.75	3.36	2.91	2.07	1.50	0.62	253/2656
TYR	0.05	1.97	3.28	1.66	1.94	1.77	1.23	0.81	17/169
ADN	-	-	-	-	-	-	-	-	0/0
ADS	0.28	-	1.14	0.75	1.10	1.04	1.67	0.83	3/20
AEG	0.16	0.10	0.09	0.66	0.63	1.01	2.00	0.83	5/58
ION	0.50	0.40	0.40	0.90	1.14	1.43	1.37	0.93	24/397
LEV	0.50	0.43	0.48	1.04	1.45	1.94	1.82	0.86	50/753
MED	0.50	0.42	0.46	1.00	1.35	1.77	1.67	0.68	412/4566

Table IV.6. Mean RMSD between nitrate model outputs and NODC-OGS dataset computed at the in situ observation locations. The metric is calculated for selected layers (0-10 m, 10-50 m, 50-100 m, 100-150 m, 150-300 m, 300-600 m, 600-1000 m), and averaged over the whole reanalysis period. Sub-basins are those of Figure III.1 or combinations of them (i.e. TYR=TYR1+TYR2; ION=ION1+ION2+ION3; LEV=LEV1+LEV2+LEV3+LEV4). The overall correlation between observations and model output is also reported with references of n. of profiles and matchups available.

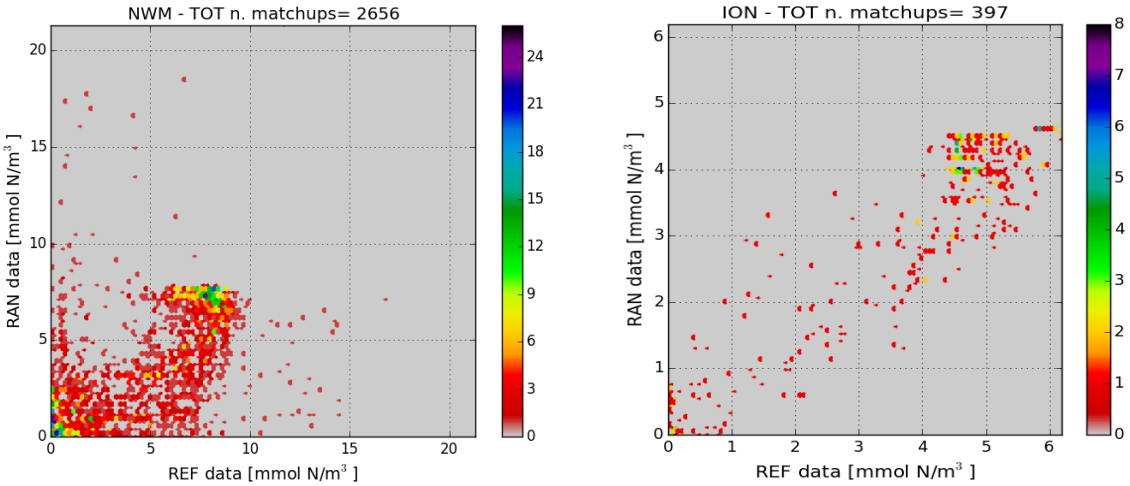

Figure IV.9. Density plots of model (RAN, y-axis) and reference (REF, x-axis) matchups of nitrate (mmol N/m^3) for ALB, NWM, LEV and ION.

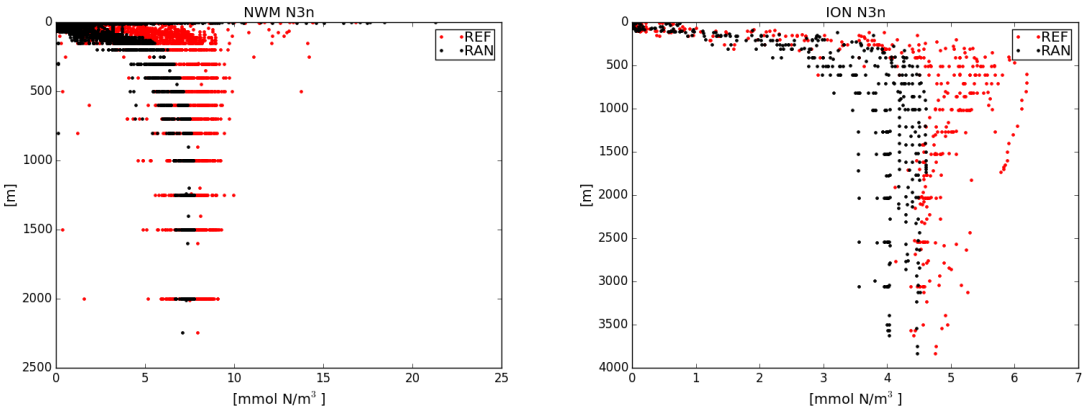

Figure IV.10. Vertical profiles of nitrate (mmol N/m^3) for reanalysis (RAN) and reference dataset (REF) for some selected sub-basins.

IV.4 Oxygen

The number of dissolved oxygen matchups is quite low (1704), almost one fifth of those available for phosphate. Thus, it is worth to remind that the kind of assessment based on the metrics of Table III.1 is very sensitive to the consistency of the observational data set considered. Therefore, the skill assessment indexes for dissolved oxygen should be considered with some caution because of the low number of available observations. No other sources of data are, at the present stage, available for an exhaustive validation of oxygen. Bio-Argo data can hopefully fill this gap in the next future, and some validation tests are already pre-operationally implemented (see http://medeaf.inogs.it/nrt-validation).

At surface (0-10 m layer), the overall basin RMSD is less than 13 mmol O_2/m^3 (Table IV.7). In general at surface, the uncertainty exceeds 15 mmol O_2/m^3 only for ALB and NWM, which can be considered a very good result, taking into account that oxygen is affected by many fast-reacting processes (i.e.: photosynthesis and respiration, and air-to-sea exchanges). A very large RMSD error is shown for the ALB sub-basin, which is three time larger of RMSD in NWM and one order of magnitude larger than most of the other sub-basins. It is worth noting that ALB, SWM1, SWM2 and NWM are those affected by the largest errors up to 150/300 m, so, even if the number of data available are in any case very few, we might suspect some incorrect setting of the Atlantic boundary conditions (see also later).

The density plots give evidence that model values be higher or lower than observations. In particular, model shows higher values and lower values than observations for low and high dissolved oxygen, respectively. In addition, statistics of Table IV.5 reveals low performances in the ALB sub-basin. This area is significantly affected by the Atlantic buffer zone, which is used as boundary condition, and where biogeochemical dynamics are not fully active (light in the buffer zone is not active). Further, the use of constant seasonal profiles as boundary condition might have generated an additional error. Therefore, oxygen in this area is affected by the uncertainty of the boundary conditions and the parameterization used at Gibraltar Strait. Errors from the boundary are then propagated to the neighbour sub-basins SWW and SWE, which show significant errors in the upper layers down to 150 m (Table IV.5).

Plots of Figure IV.12 show that the model is consistent with the oxygen dynamics affecting the shape of the vertical profiles. Sub-basin correlations are, indeed, high and significant (larger than 0.73, except ALB, SWW and AEG, Table IV.5). Further, a subsurface minimum in the observations (at around 500 m) appears not reproduced in model results in some sub-basins with differences of about 10 mmol O_2/m^3 (see for example Figure IV.12 for ION and LEV, while for NWM the minimum is around 250 m and the overestimation is about 20 mmol O_2/m^3).

	RMSD							CORR.	n. of profiles/matchups
	0-10	10-50	50-100	100-150	150-300	300-600	600-1000		
ALB	101.7	121.4	124.9	86.41	21.74	21.91	15.53	-0.48	6/83
SWM1	14.65	32.86	36.45	39.03	23.64	17.88	14.29	0.37	6/109
SWM2	11.77	17.35	37.76	23.27	16.97	25.85	16.51	0.73	4/83
NWM	28.91	27.97	18.54	13.18	17.75	18.38	10.82	0.81	10/189
TYR	14.00	23.55	17.34	10.94	14.03	17.60	14.84	0.90	10/160
ADN	-	-	-	-	-	-	-	-	0/0
ADS	14.32	14.27	13.55	14.00	8.32	2.73	6.29	0.96	3/39
AEG	11.22	15.79	18.03	15.29	11.18	10.44	14.08	0.42	5/81
ION	13.44	17.07	19.28	14.27	7.79	9.22	9.80	0.88	19/338
LEV	12.35	17.81	18.58	17.34	12.12	12.63	12.66	0.78	33/622
MED	12.93	17.57	18.86	16.36	10.58	11.51	11.69	0.47	96/1704

Table IV.7. Mean RMSD between dissolved oxygen model outputs and NODC-OGS dataset computed at the in situ observation locations. The metric is calculated for selected layers (0-10 m, 10-50 m, 50-100 m, 100-150 m, 150-300 m, 300-600 m, 600-1000 m), and averaged over the whole reanalysis period. Sub-basins are those of Figure III.1 or combinations of them (i.e. TYR=TYR1+TYR2; ION=ION1+ION2+ION3; LEV=LEV1+LEV2+LEV3+LEV4). The overall correlation between observations and model output is also reported with references of n. of profiles and matchups available.

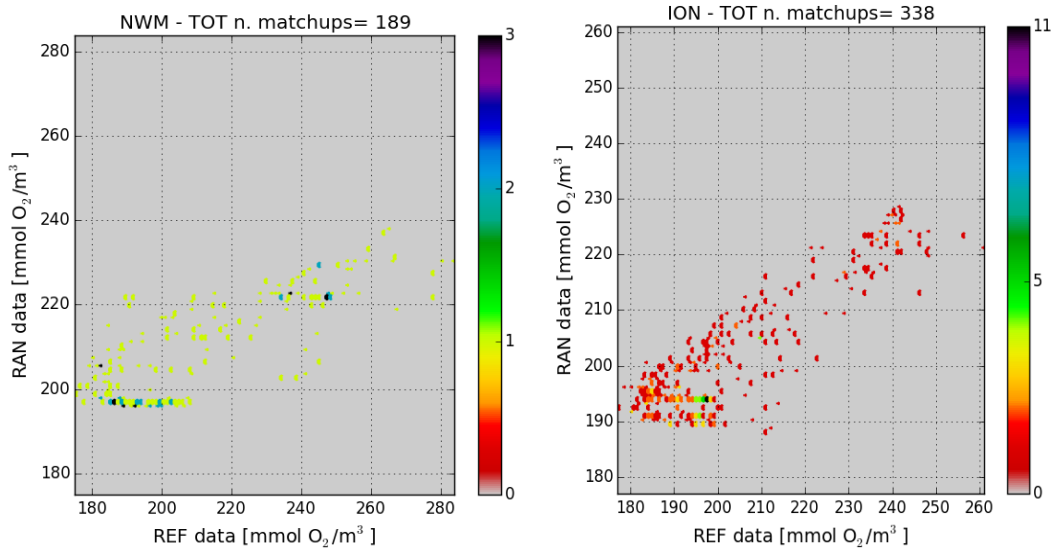

Figure IV.11. Density plots of model (RAN, y-axis) and reference (REF, x-axis) matchups of dissolved oxygen (mmol O_2/m^3) for ALB, NWM, ION and LEV.

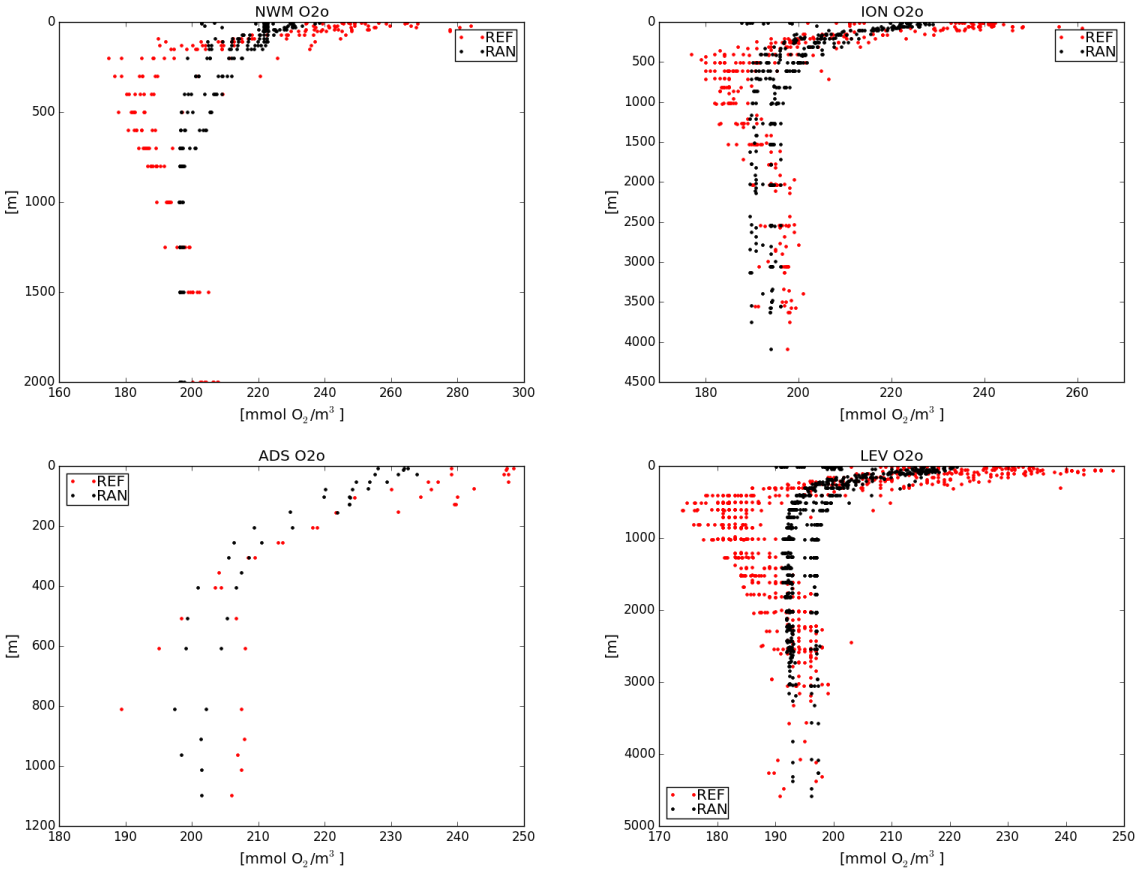

Figure IV.12. Vertical profiles of dissolved oxygen (mmol O_2/m^3) for reanalysis (RAN) and reference dataset (REF) for some selected sub-basins.

IV.5 pH and pCO2

Dataset CARB, which includes pH (ocean acidity) and pCO2 (partial pressure of carbon dioxide in sea water), has been validated using an indirect estimate. The data available of pH and pCO2 are too scarce (less than 30% of the datasets of Table III.3 contain pH) and it is unfeasible either to compute quantitative skill validation metrics or to extract a reliable climatology for qualitative comparison. Therefore, the accuracy of pCO2 (U_{pCO2}) and pH (U_{pH}) is estimated starting from the accuracy of DIC (U_{DIC}) and alkalinity (U_{alk}) and adopting a propagation error approach.

Dissolved inorganic carbon (DIC) and alkalinity (ALK) are the prognostic variables (state variables) of the carbonate system of the BFM model. Moreover, they are the carbonate system variables with the largest number of observations (up to 90% of the datasets of Table III.3).

Considering the historical observations, two kinds of climatological reference datasets have been computed: mean annual climatological map at 1°x1° of resolution, and mean profiles computed over 18 selected areas 4°x4° wide (see section III for additional explanations).

Reanalysis results (January 1999 – December 2016) are then used to compute the corresponding averages at the same temporal and spatial discretization of the climatology derived by the observations, in order to compare DIC and alkalinity.

The results of the comparison with the 1°x1° climatology maps (Figure IV.13 and 14) indicate a significant good agreement of the main basin wide characteristics. In particular, a strong west-to-east surface gradient of both alkalinity and DIC is the main spatial pattern that can be recognized both on reanalysis and climatology maps. The eastern marginal seas (Adriatic and Aegean Seas) are characterized by the highest values. The west-to-east gradient is a permanent structure recognizable at all depths, but less marked in the maps of the intermediate and deep layers (see for example the layer 200-500, Figure IV.14). At the surface, DIC and alkalinity dynamics are driven by three major factors: the input in the eastern marginal seas (the terrestrial input from the Po and other Italian rivers and the input from the Dardanelles), the effect of evaporation in the eastern basin and the influx of the low-alkaline ad low-DIC Atlantic waters. The thermohaline basin-wide circulation modulates the intensity and the patterns of the spatial gradients. Intermediate and deep layers show weaker dynamics and less variability.

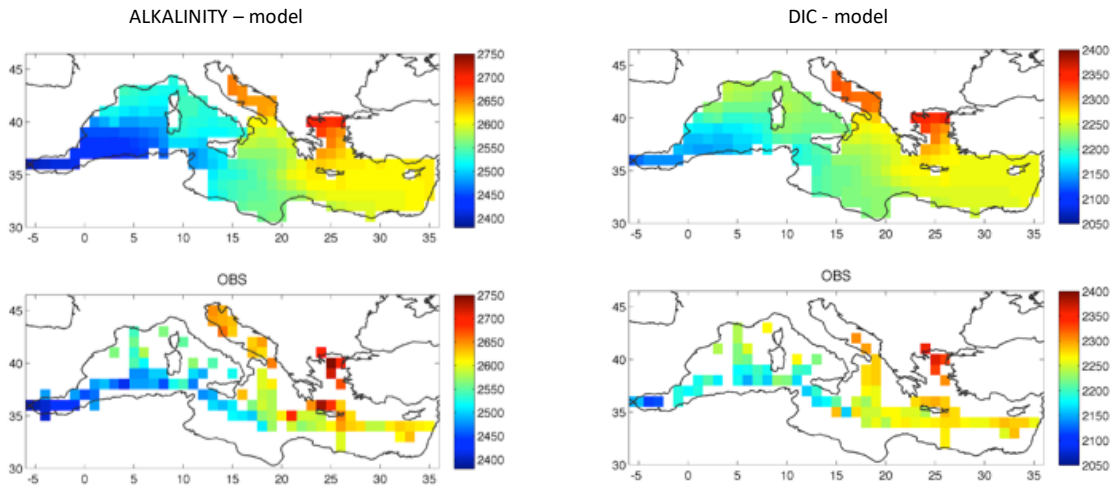

Figure IV.13. Mean annual map of Alkalinity (left) and DIC (right) of the reanalysis (upper panels) and reconstructed by the 1°x1° climatology (lower panels) for the layer 0-50 m.

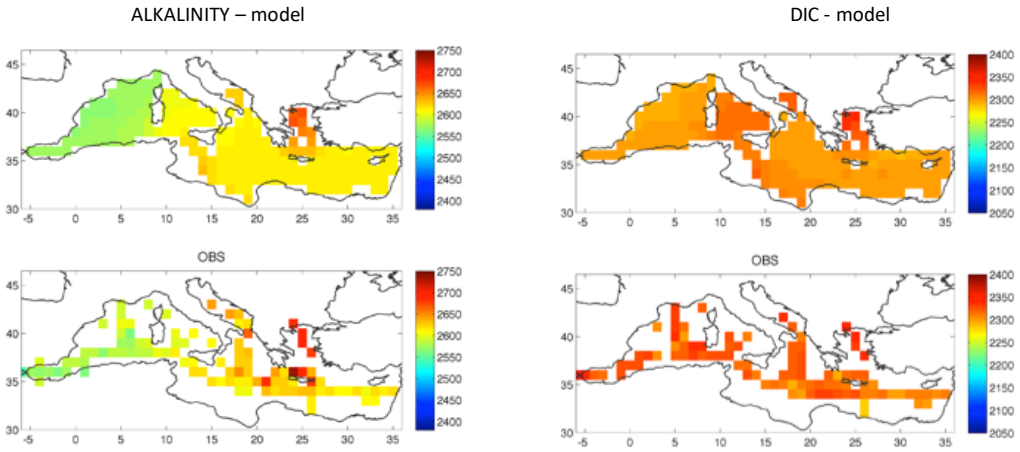

Figure IV.14. Mean annual map of Alkalinity (left) and DIC (right) of the reanalysis (upper panels) and reconstructed by the 1°x1° climatology (lower panels) for the layer 200-500 m.

The skill performance was analysed by computing the correlation, the bias and the root mean square of the differences (RMSD) between the mean model maps and the 1°x1° climatology maps for the selected layers. Model results have been mapped on the observational space by computing the spatial averages at 1° of resolution and by computing the temporal average for the period of the reanalysis run. The results of the skill metrics, reported in Table IV.8, show that correlations are significant and very high for both variables at the surface layer. The correlations of alkalinity are always higher than 0.7 in all layers. DIC correlations decrease with depth because model maps of DIC below 200 m are characterized by very low gradients from east to west, while the climatological maps feature rather fuzzy patterns. The mean BIAS error is around 8 and 11 µmol/kg for alkalinity and DIC, respectively, while the mean RMSD, which is used as the estimate of the accuracy, is about 20 µmol/kg for both variables.

	Alkalinity			DIC		
Layer depth	**BIAS**	**RMSD**	**CORR**	**BIAS**	**RMSD**	**CORR**
0-50	-7.0	24.2	0.92	-8.4	20.9	0.89
50-100	-10.8	26.5	0.85	-10.3	22.9	0.64
100-150	-8.1	22.5	0.85	-13.1	26.9	0.36
150-200	-6.2	18.3	0.78	-10.9	26.2	0.28
200-500	-5.5	13.7	0.81	-15.1	19.5	0.31
500-1500	-6.1	14.5	0.73	-9.7	14.4	-0.17
1500-4000	-13.4	17.5	0.70	-14.0	16.7	-0.20

Table IV.81. Skill metrics for the comparison of alkalinity and DIC on the 1x1 grid domain and selected layers.

The performance of the carbonate system variables DIC and alkalinity is also evaluated by computing the skill metrics on vertical profiles of 18 selected areas defined in Figure III.3. Examples of the comparison between mean model profiles and the climatological profiles are given in Figure IV.15 and

IV.16 while the skill metric values are given in Table IV.7. The analysis of the figures confirms the satisfactory skill of the model in reproducing the shapes of the profiles and the distribution of vertical values along the west to east gradient for both variables. It is worth to note that, given the rather poor available information and data, the CMEMS-MED-MFC-Biogeochemistry model system presents a good capability to reproduce the average conditions of the carbonate system variables at the basin scale. The correlations of alkalinity and DIC are very high and significant for most of the areas, where observations are enough to build a consistent and reliable profile. In some areas (i.e. areas 9, 11, 12, 13, 14 and 15 and 18 for alkalinity, and 12 for DIC) observations are scarce in several layers and the profile is not consistent. For example, plots of areas 13 and 15 for alkalinity (Figure IV.15) show observation profiles characterized by scattered values. Correlation in this area is not a reliable metric to be used for validation, however, the plots and the other skill metrics show that reanalysis values are well within the interval of variability of the data.

The average BIAS and RMSD over the 18 areas are -7.8 and 19.0 µmol/kg and -11.9 and 17.2 µmol/kg for alkalinity and DIC respectively. These values are even better than those computed for the horizontal maps.

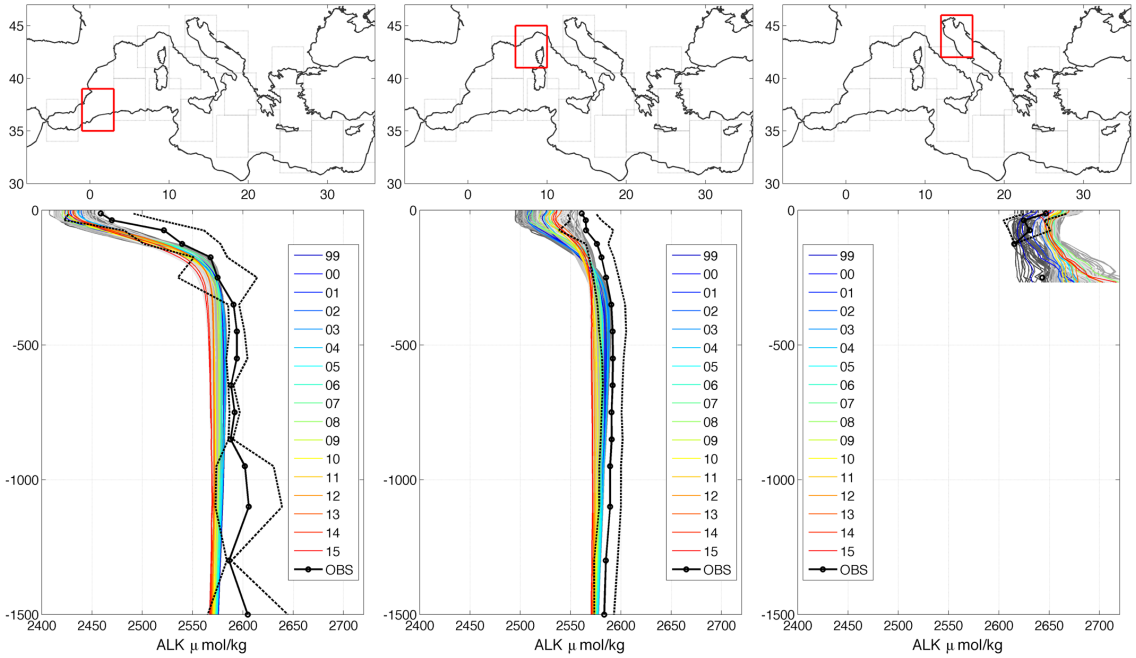

Figure IV.15. Alkalinity profiles: mean monthly model profiles (grey color lines; from January 1999 to December 2015), mean annual model profiles (colour scale lines) and climatological (±standard deviation) profiles (black lines) for the areas 2, 6, 9, 13, 15 and 18 of Figure III.3 (continues overleaf).

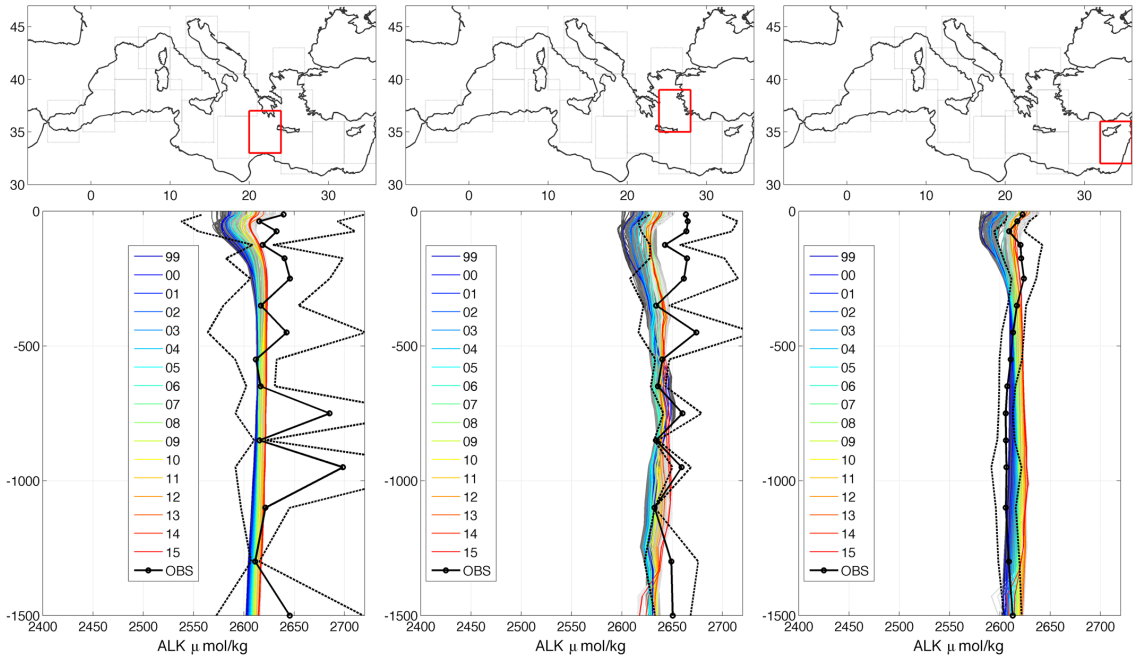

Figure IV.15. (continued) Alkalinity profiles: mean monthly model profiles (grey color lines; from January 1999 to December 2015), mean annual model profiles (colour scale lines) and climatological (±standard deviation) profiles (black lines) for the areas 2, 6, 9, 13, 15 and 18 of Figure III.3.

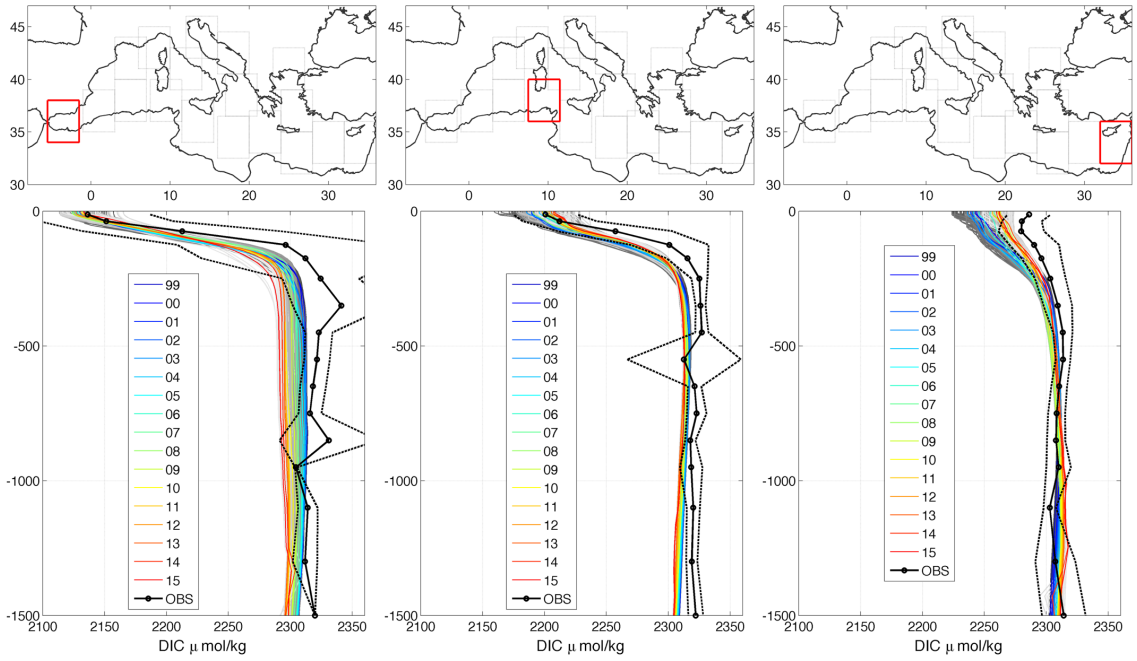

Figure IV.16. DIC profiles: mean monthly model profiles (grey color lines; from January 1999 to December 2015), mean annual model profiles (colour scale lines) and climatological (±standard deviation) profiles (black lines) for the areas 1, 5, 18 of Figure III.3.

	Alkalinity			DIC		
Areas	BIAS	RMS	CORR	BIAS	RMS	CORR
1	-5.7	15.4	0.97	-19.7	23.7	0.98
2	-23.0	25.3	0.98	-28.6	31.7	0.97
3	-9.5	13.7	0.97	-15.2	18.0	0.98
4	-21.5	23.3	0.91	-18.3	20.2	0.94
5	-5.2	8.6	0.98	-13.3	16.0	0.97
6	-16.5	19.1	0.97	-23.6	26.2	0.92
7	6.2	9.7	0.99	-4.1	11.4	0.98
8	-6.6	11.3	0.94	-6.2	11.2	0.95
9	24.9	27.0	0.58			
10	-4.7	9.0	0.93	-5.5	8.5	0.98
11	-18.5	25.1	0.09	-13.0	15.6	0.87
12	-6.2	16.9	-0.43	-17.4	22.6	-0.14
13	-21.7	31.2	0.25	-9.5	12.9	0.86
14	-9.1	13.3	0.06	-10.0	12.1	0.93
15	-22.3	28.6	0.03	-13.4	14.6	0.91
16	-3.2	47.7	0.21	9.8	24.6	0.74
17	-0.4	6.7	0.15	-8.4	10.5	0.93
18	1.7	9.2	-0.11	-6.5	12.4	0.92

Table IV.9. Skill metrics of the comparison of alkalinity and DIC on the 18 selected areas 4°x4° wide.

The CARB variables, ocean acidity (pH) and ocean pCO2, are essential climate variables (ECVs) and are commonly used in the UNFCCC and IPCC reports as indicators of the climate change and the ocean acidification processes. These variables are affected by the climate change (acidification) trends and by the natural variability within the marine ecosystem due to the many physical and biological processes that influence DIC, alkalinity and temperature. As an example of the variability of the annual cycle, the February, May, August and November climatological maps of pH and pCO2 at surface are given in Figure IV.17 and IV.18. The climatological map of a given month (e.g. February) is computed by averaging all the February months within the reanalysis period 1999-2015. We can observe that pH and pCO2 exhibit spatial patterns partly overlapped to those of DIC and alkalinity and partly connected to the temperature dynamics due to the thermal effect on the activity of $[H^+]$ and on the CO2 solubility. Indeed, the monthly maps depict a variability of the annual cycle that is as high as 0.15-0.20 and 150-200 ppm for pH and pCO2, respectively.

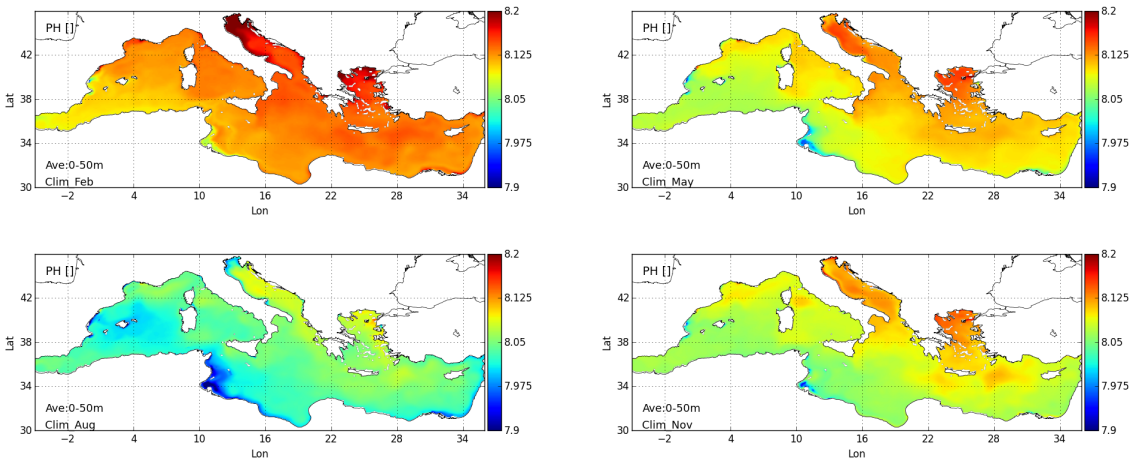

Figure IV.17. Climatological monthly values of pH at in situ condition and reported on Total Scale at the 0-50 m layer for February, May, August and November. A climatological map of a given month is computed by considering all the given months within the period of the reanalysis 1999-2015.

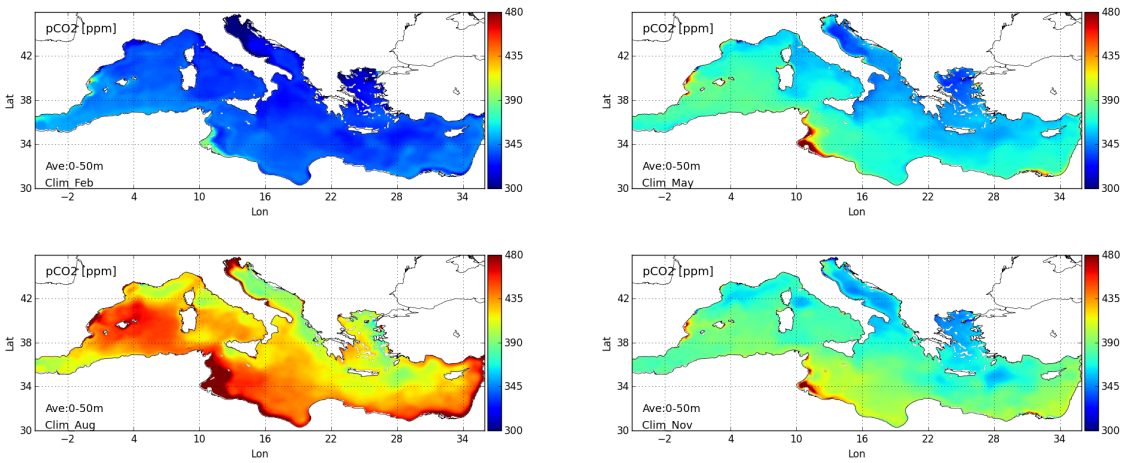

Figure IV.18. Climatological monthly values of pCO2 [ppm] at the 0-50 m layer for February, May, August and November. A climatological map of a given month is computed by considering all the given months within the period of the reanalysis 1999-2015.

As previously mentioned, the quality assessment of the CARB variables pH and pCO2 is based on an indirect estimate. The accuracy of pCO2 (U_{pCO2}) and pH (U_{pH}) is estimated starting from the accuracy of DIC (U_{DIC}) and alkalinity (U_{alk}) adopting the following propagation error approach:

$$U_{pCO2} = ((\frac{\delta pCO2}{\delta DIC} \cdot U_{DIC})^2 + (\frac{\delta pCO2}{\delta alk} \cdot U_{alk})^2)^{0.5}$$

$$U_{pH} = ((\frac{\delta pH}{\delta DIC} \cdot U_{DIC})^2 + (\frac{\delta pH}{\delta alk} \cdot U_{alk})^2)^{0.5}$$

Using the results of the comparison on the 1°x1° maps, the RMS of DIC and alkalinity, reported in Table IV.6, is assumed as the measure of their uncertainty. The derivatives of pCO2 and pH with respect to

DIC and alkalinity are approximated by their local numerical deviations. Then, the resulting uncertainties of the mean values of pCO2 and pH at the surface layer are:

U_{pCO2}= 48.1 ppm

U_{pH}= 0.0477

These are conservative estimates of the uncertainty of pH and pCO2. First, it is worth to note that DIC and alkalinity are, to some degree, correlated variables (see Figures IV.13 and IV.14) since some processes have similar impacts on both variables. Indeed, an underestimation of DIC is likely to occur with an underestimation of alkalinity (e.g. an error on the dilution – concentration process at surface has the same impact on both variables). Then, DIC and alkalinity have an opposite effect on pH and pCO2 (Zeebe and Wolf-Gladrow, 2001). Therefore, considering a concomitant overestimation / underestimation of DIC and alkalinity, it is presumable to assume that the error estimate of pH and pCO2 does not increase with the sum of the errors of the two variables. Further, the choice of using the basin-wide RMS estimate as the measure of the uncertainty might have given an overestimation of the total uncertainty. Indeed, the highest model-climatology errors are computed in transitional areas between sub-basins and in marginal areas. DIC and alkalinity uncertainties computed at sub-basin scale (e.g. values of statistics on 4°x4° climatology) would have had lower values. However, since the low availability of data, the estimates would also be less reliable.

V SYSTEM'S NOTICEABLE EVENTS, OUTAGES OR CHANGES

Date	Change/Event description	System version	other
5/03/2016	First release of Mediterrean Sea biogeochemical reanalysis at 1/16 including carbonate system variables for the period 1999-2014	MedBFM0	V2 version
16/04/2017	Upgrade of data assimilation scheme including satellite chlorophyll over the entire domain (both coastal and open sea areas), re-run of the whole period 1999-2014 and extension of one year (2015)	MedBFM1	V3 version
18/04/2018	Extension of one year (2016)	MedBFM1	V4 version
16/04/2019	Extension of one year (2017)	MedBFM1	Q2 2019
3/09/2019	Extension of one year (2018)	MedBFM1	Q4 2019

VI QUALITY CHANGES SINCE PREVIOUS VERSION

The biogeochemical MedBFMv1 model system coupled with the physical MFSe1r1 model system has provided the 1999-2015 reanalysis in Q2/2016 and the subsequent time series extensions for the years 2016, 2017 and 2018 in Q2/2018, Q2/2019 and Q4/2019, respectively. The reanalysis differs from the previous one (released in 2015) for the upgrade of the data assimilation scheme (i.e., assimilation of surface chlorophyll over the entire Mediterranean domain including the coastal areas). A quality assessment of the reanalysis products in the coastal area has been provided for the first time, showing significant improvements for the chlorophyll and small improvements for nutrients. There are basically no changes in the quality of the open sea area of the Mediterranean Sea for the datasets NUTR, BIOL, PFTC., and CARB.

VII REFERENCES

• Artuso F., Chamard P., Piacentino S., Sferlazzo D.M., De Silvestri L., di Sarra A., Meloni D., Monteleone F., 2009. Influence of transport and trends in atmosphericCO2at Lampedusa. Atmos. Environ. 43 (19), 3044–3051.

• Bergametti G., Remoudaki E., Losno R., Steiner E., Chatenet B., 1992. Source, transport and deposition of atmospheric Phosphorus over the northwestern Mediterranean, J. Atmos. Chem., 14, 501–513.

• Bethoux, J. P., Morin, P., Chaumery, C., Connan, O., Gentili, B., and Ruiz-Pino, D., 1998. Nutrients in the Mediterranean Sea, mass balance and statistical analysis of concentrations with respect to environmental change, Mar. Chem., 63, 155–169.

• Copin-Montegut C., 1993. Alkalinity and carbon budgets in the Mediterranean Sea. Global Biogeochemical Cycles, 7(4), pp. 915-925.

• Cornell S., Rendell A., Jickells T., 1995. Atmospheric inputs of dissolved organic Nitrogen to the oceans, Nature, 376, 243–246.

• Cossarini G., Lazzari P., Solidoro, C., 2015. Spatiotemporal variability of alkalinity in the Mediterranean Sea. Biogeosciences, 12(6), 1647-1658.

• Crise, A., Solidoro, C., and Tomini, I.: Preparation of initial conditions for the coupled model OGCM and initial parameters setting, MFSTEP report WP11, subtask 11310, 2003.

• Dobricic S., Pinardi N., 2008. An oceanographic three-dimensional variational data assimilation scheme. Ocean Modelling, 22, 3-4, 89-105.

• Foujols, M.-A., Lévy, M., Aumont, O., Madec, G., 2000. OPA 8.1 Tracer Model Reference Manual. Institut Pierre Simon Laplace, pp. 39.

• Guerzoni, S., Chester, R., Dulac, F., Herut, B., Loÿe-Pilot, M.-D., Measures, C., Migon, C., Molinaroli, E., Moulin, C., Rossini, P., Saydam, C., Soudine, A., Ziveri, P., 1999. The role of atmospheric deposition in the biogeochemistry of the Mediterranean Sea. Prog. Oceanogr., 44 (1-3): 147-190.

• Herut, B. and Krom, M.: Atmospheric input of nutrients and dust to the SE Mediterranean, in: The Impact of Desert Dust Across the Mediterranean, edited by: Guerzoni, S. and Chester, R., Kluwer Acad., Norwell, Mass., 349–358, 1996.

• Krom M.D., Kress N., Brenner S., Gordon L.I., 1991. Phosphorus limitation of primary productivity in the eastern Mediterranean Sea. Limnology and Oceanography, 36(3) 424-432.

• Lazzari P., Teruzzi A., Salon S., Campagna S., Calonaci C., Colella S., Tonani M., Crise A., 2010. Pre-operational short-term forecasts for the Mediterranean Sea biogeochemistry. Ocean Science, 6, 25-39.

• Lazzari, P., Solidoro, C., Ibello, V., Salon, S., Teruzzi, A., Béranger, K., Colella, S., and Crise, A., 2012. Seasonal and inter-annual variability of plankton chlorophyll and primary production in the Mediterranean Sea: a modelling approach. Biogeosciences, 9, 217-233.

• Lazzari, P., Solidoro, C., Salon, S., Bolzon, G., 2016. Spatial variability of phosphate and nitrate in the Mediterranean Sea: a modelling approach. Deep Sea Research I, 108, 39-52.

• Loÿe-Pilot M. D., Martin J. M., and Morelli J., 1990. Atmospheric input of inorganic nitrogen to the western Mediterranean. Biogeochem., 9: 117-134.

• Ludwig W., Dumont E., Meybeck M., Heussner S., 2009. River discharges of water and nutrients to the Mediterranean and Black Sea: Major drivers for ecosystem changes during past and future decades?. Prog. Oceanogr., 80 (3-4): 199-217.

• Orr J.C., Najjar R., Sabine C.L., Joos F., 1999. Abiotic-HOWTO. Internal OCMIP Report, LSCE/CEA Saclay, Gifsur-Yvette, France, 25 pp.

• Ribera d'Alcalà M., Civitarese G., Conversano F., Lavezza R., 2003. Nutrient ratios and fluxes hint at overlooked processes in the Mediterranean Sea. Journal of Geophysical Research, 108(C9), 8106, doi:10.1029/2002JC001650.

• Somot S., Sevault F., Déqué M., Crépon M., 2008. 21st century climate change scenario for the Mediterranean using a coupled atmosphere–ocean regional climate model, Global and Planetary Change, 63, 2–3: 112–126.

• Teruzzi A., Dobricic S., Solidoro C., Cossarini G., 2014. A 3D variational assimilation scheme in coupled transport biogeochemical models: Forecast of Mediterranean biogeochemical properties, Journal of Geophysical Research, doi:10.1002/2013JC009277.

• Teruzzi A., Bolzon G., Salon S., Lazzari P., Solidoro C., Cossarini G., 2018. Assimilation of coastal and open sea biogeochemical data to improve phytoplankton simulation in the Mediterranean Sea. Ocean Modelling, https://doi.org/10.1016/j.ocemod.2018.09.007 2018

• Teruzzi A., Di Cerbo P., Cossarini G., Pascolo E., Salon S., 2019. Parallel implementation of a data assimilation scheme for operational oceanography: The case of the MedBFM model system. Computers & Geosciences, https://doi.org/10.1016/j.cageo.2019.01.003

• Thingstad T.F., Rassoulzadegan F., 1995. Nutrient limitations, microbial food webs, and 'biological C-pumps': suggested interactions in a P-limited Mediterranean. Marine Ecology Progress Series, 117: 299-306.

• World Ocean Atlas 2013 database, https://www.nodc.noaa.gov/OC5/woa13/

• Zeebe R.E. and Wolf Gladrow D., 2001. CO2 in seawater: equilibrium, kinetics, isotopes, Elsevier oceanography series. Elsevier.